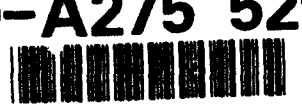

(2)

Tunnelling Hot Electron Transfer Amplifiers: Final Report Contract N00014-87-C-0709

C.J. Kircher (for M. Heiblum)

October 30, 1993

IBM Research Division
T. J. Watson Research Center
Yorktown Heights, New York 10598

IBM

34pgs

Significant advances were achieved in tunneling hot electron amplifiers and in the understanding of hot electron transport in the work funded by the contract and carried out by M. Heiblum and his co-workers.# This results of this work are described in detail in nine papers that have been published in the open literature. (These papers are listed below as references 1-9 and copies of them are attached.) This report summarizes the principal results.

There are three aspects of the work in which the results are particularly noteworthy:

1. The demonstration of the first hot hole tunneling transistor and its use to study hot hole transport in GaAs,
2. The successful fabrication of a hot electron "THETA" transistor with a psuedomorphic InGaAs base which allowed high transistor gains ($\beta \sim 30$) to be achieved, and
3. The conception and successful fabrication of a lateral hot electron device and its use to investigate ballistic, hot electron transport in a 2-dimensional electron gas in GaAs.

Hot Hole Tunneling Transistor[1]

The first operation of a tunnelling hot hole transfer amplifier was demonstrated and spectroscopic evidence of ballistic light hole transport was observed. Light holes can be separated from the majority of the heavy ones by tunnelling which favors the light holes due to the mass difference. Thus, a tunnelling barrier was used as an injector of light hot holes into a p-type, 30nm-thick GaAs base layer. Energy spectroscopy was performed at the exit of the layer by using a 46 nm wide AlGaAs collector barrier. Narrow energy distributions of hot holes were detected with width of about 35 meV and with peak energies corresponding to the injection energies at the entrance to the layer, confirming ballistic transport. The fraction of the holes travelling ballistically (i.e., without scattering or energy loss) is about 10% for holes injected at energies 180-220 meV, suggesting a mfp in $2x10^{18}$ cm^{-3} p-type GaAs of about 14 nm. This is about three times smaller than the mean free path of electrons in n-type GaAs doped to the same level.

By applying a magnetic field perpendicular to the direction of ballistic hole motion, thus deflecting the holes from their original straight trajectories via the Lorentz force, it was demonstrated that one can estimate the effective mass of the hot holes and thus their velocity. Analysis of the data using a simple model suggests that the light holes injected 0.22 eV below the top of the valence band have a mass of about 0.15 m_e, where m_e is the free electron mass (at the top of the valance band their mass would be about 0.082 m_e), and a group velocity of about $6.5x10^7$ cm/sec. This value is $\sim$ 10x faster than that of heavy holes in GaAs and approaching the value of $\sim$ $10x10^7$ cm/sec for hot electrons. Hot light-hole THETA devices should thus have performance potential approaching that of similar hot electron devices.

Hot Electron Transistor with Psuedomorphic InGaAs Base[4,6]

An AlGaAs/InGaAs/AlGaAs pseudomorphic base structure can be incorporated in the THETA device. The use of the strained InGaAs layer as the base material increases the energy separation between conduction band Γ and L-valleys of the base region, and enables the use of a lower aluminum mole fraction in the AlGaAs collector barrier for the same base-collector leakage current. As a result, two factors limiting the current gain in THETA device, hot-electron transfer into the L-valleys in the base and scattering of hot-electrons in the AlGaAs collector barrier, can be reduced.

Successful fabrication of the first pseudomorphic base THETA devices was achieved. Ballistic electron transport was observed using hot electron spectroscopy. From collector current onsets and activation energy measurements, it was found (assuming no charge in the AlGaAs) that the conduction band discontinuity, ΔE_c, between strained $In_{0.15}Ga_{0.85}As$ and $Al_{0.15}Ga_{0.85}As$ increases by about

100 meV compared to that of the GaAs - $Al_{0.15}Ga_{0.85}As$ interface. Also a slight decrease in the current gain α at high base-emitter voltage is observed, which suggests that Γ-L valley energy separation in $In_{0.15}Ga_{0.85}As$ is about 400 meV compared to 290 meV in GaAs.

These increased energies result in significant increases in transistor gain: Common emitter current gains of 25-30 at 77 K and 35-40 at 4.2 K were obtained. These values are about 4x higher than in devices with GaAs bases having similar thickness and doping and correspond to a transfer ratio in a common base operation of about 0.97, suggesting that a very large fraction of the electrons traverse the device with negligible energy loss. This is a significant advance since these gains are reaching the range that would be needed for practical devices.

Lateral Ballistic Electron Transistor[8,9]

The first lateral ballistic hot electron transistors have been constructed. In these devices, transport occurs in the plane of a high mobility two dimensional electron gas (2 DEG) at a GaAs/AlGaAs heterojunction. The device is formed by the deposition of two metal gates, 50 nm long, and 0.5 microns wide, separated by 50 nm on the surface over the 2DEG. With an applied negative voltage to both gates with respect to the 2DEG, the electron density underneath the two gates is reduced to zero and two potential barriers are induced. The two barriers separate the 2DEG into three different regions: an emitter, base (center region), and collector to which separate ohmic contacts are made. The emitter barrier, separating the emitter from the base, is used as a tunnelling injector of a quasi monoenergetic beam of hot electrons. The hot electrons, with excess energy of 30-100 meV above the Fermi level traverse the base (in the plane of the 2 DEG) and surmount the second induced barrier, the collector barrier, to be collected. The principles of operation are the same as for the vertical THETA device but, the lateral device is easier to make and very flexible in its operation. For example, ohmic contacts to the base can be readily made and the gates enable the potential barriers to be adjusted to optimize the operation of the device. Lateral devices also offer some new device possibilities: For example, it should be possible to steer electrons in the plane of the 2DEG and to integrate lateral hot electron devices with conventional HFET structures.

Several types of lateral devices were fabricated. They were used to verify the tunnelling behavior of the injector, to investigate the sensitivity of the current transfer ratio α to the design of the emitter and collector gates, and to carry out electron energy spectroscopy experiments in order to investigate the conditions under which ballistic transport can occur. From the lattermost, phonon scattering was found to be the primary scattering mechanism in these devices. At base lengths of $\sim$ 1μm (significantly greater than the mean-free-path for phonon scattering in GaAs), the spectroscopy results show clear evidence of phonon scattering at multiples of 36meV (the phonon energy in GaAs). For transistors with a base length of 220 nm (approximately equal to the mfp), electron transport was shown to occur without electron scattering, i.e., it was mainly ballistic. For devices of this base length having gate electrodes designed for gain improvement, it was possible to achieve very high current gains - as large as α = 0.99 (β = 100) at 4.2K.

Note: M. Heiblum no longer works for IBM. C.J. Kircher was his manager during much of the contract period.

References

1. M. Heiblum, K. Seo, H. P. Meier, and T. W. Hickmott, "Observation of Ballistic Holes," Phys. Rev. Lett. **60**, 828 (1988).

2. H. Shtrikman, M. Heiblum, K. Seo, D. Galbi, and L. Osterling, "High Mobility Inverted Selectively Doped Heterojunctions," J. Vac. Sci. Tech. B **6**, 670 (1988).

3. U. Meirav, M. Heiblum, and F. Stern, "High Mobility Variable Density Two Dimensional Electron Gas in Inverted GaAs-AlGaAs Heterojunctions," Appl. Phys. Lett. **52**, 1268 (1988).

4. K. Seo, M. Heiblum, C. M. Knoedler, W-P. Hong, and P. Bhattacharya, "Pseudomorphic InGaAs Base Ballistic THETA Device," Appl. Phys. Lett. **53**, 1946 (1988).

5. M. Heiblum, D. Galbi, and M. Weckwerth, "Observation of a Single Phonon Emission," Phys. Rev. Lett. **62**, 1057 (1989).

6. K. Seo, M. Heiblum, C. M. Knoedler, J. Oh, J. Pamulapati, and P. Bhattacharya, "High Gain Pseudomorphic InGaAs Base Ballistic Hot Electron Device," Electron Dev. Lett. **10**, 73 (1989).

7. C. M. Knoedler, L. Osterling, and M. Heiblum, "Inert Gas Reactive Ion Damage to GaAs/AlGaAs Inverted Heterojunctions," J. Appl. Phys. **65**, 1800 (1989).

8. A. Palevski, M. Heiblum, C. P. Umbach, C. M. Knoedler, A. N. Broers, and R. H. Koch, "Lateral Tunnelling, Ballistic Transport, and Spectroscopy in a Two-Dimensional-Electron-Gas," Phys. Rev. Lett. **62**, 1776 (1989).

9. A. Palevski, C. P. Umbach, and M. Heiblum, "A High Gain Lateral Hot Electron Device," Submitted to Appl. Phys. Lett.

Observation of Ballistic Holes

M. Heiblum,[1] K. Seo,[1] H. P. Meier,[2] and T. W. Hickmott[1]

[1]*IBM Research Division, T. J. Watson Research Center, Yorktown Heights, New York 10598*

[2]*IBM Research Division, Zurich Research Laboratory, 8803 Rüschlikon, Switzerland*

(Received 13 November 1987)

We report the first direct observation of ballistic hole transport in semiconductors, via energy spectroscopy experiments. Light holes are preselected and injected via tunneling into 31-nm-thick p^+-GaAs layers. About 10% of the injected holes have been found to travel ballistically maintaining distributions $\simeq$35 meV wide, with a mean free path of about 14 nm. Resonances in the injection currents, resulting from quantum interference effects of the ballistic holes, are used to support the light nature of the ballistic holes.

PACS numbers: 72.20.Jv, 71.25.Tn, 73.40.Gk

Ballistic transport of carriers in solids was previously inferred via a variety of indirect techniques.[1-3] Recent energy spectroscopy experiments in GaAs have demonstrated directly the existence of ballistic electrons[4]; however, holes were never directly observed to be transported ballistically. In GaAs there are two valence bands[5]: a light-hole band containing about 5% of the total hole population, with a curvature effective mass $m_{lh}=0.082m_e$, where m_e is the free-electron mass, and a heavy-hole band with $m_{hh}=0.51m_e$. Since the mean free path (mfp) is approximately proportional to the inverse of the mass, ballistic transport of heavy holes is unlikely in practical structures. In order to look for ballistic hole transport we have used a tunnel barrier, which has large transmission for light holes, injecting $\simeq$30-meV-wide energy distributions of light holes into heavily doped p^+-GaAs layers, 31 nm thick. With spectroscopy performed after traversal, we have measured similar distribution widths and peak energies, with about 10% of the holes being ballistic. The ballistic transport and the light nature of the holes are supported by the observation of resonances in the injection currents due to quantum interference effects of the ballistic light holes in the thin GaAs layers.[6]

Experiments were done with a novel three-terminal structure (hot-hole transistor) grown by molecular-beam epitaxy on a p^+ (100) GaAs substrate, described in Fig. 1. A tunnel injector, composed of a p^+-GaAs layer (called emitter), an intrinsic $Al_xGa_{1-x}As$ barrier layer with $x=0.5$ (12 nm thick), and a p^+-GaAs layer (31 nm thick, called base), was used to select and inject light holes. When biased with V_{EB} it injected a quasimonoenergetic distribution of light hot holes ($\simeq$30 meV wide), favored by the tunneling process (by a factor of $\simeq10^7$), with most holes emerging into the base layer with excess energy near eV_{EB}. The 31-nm base layer was terminated with a spectrometer made of a relatively thick, intrinsic $Al_yGa_{1-y}As$ layer with $y=0.31$ (47 nm thick, called collector barrier), followed by a thick p^+-GaAs layer (called collector). The AlAs mole fraction in the collector barrier was linearly graded down to $y=0.17$ over 6 nm on the base side to minimize the quantum-mechanical reflections. The GaAs layers were doped with acceptors (Be) to a level of 1.6×10^{18} cm^{-3}. The structure was selectively etched to expose the base layer, and alloyed Ohmic contacts were made to the emitter, base, and collector layers.

Arriving hole distributions were analyzed by the thick AlGaAs spectrometer barrier. Upon the application of a potential difference, V_{CB}, the potential height of the collector barrier, Φ_C, changes, affecting the collected current density $J_C=e\int_{\Phi_C}^{\infty}n(E_\perp)v_\perp(E_\perp)dE_\perp$, where e is the electronic charge, and $n(E_\perp)$ is the number of holes per unit normal energy, an energy associated with the normal component of the velocity, $v_\perp(E_\perp)$. The normal energy distribution can be found from $ev_\perp(E_\perp)n(E_\perp)=dJ_C/d\Phi_C$, or

$$v_\perp(E_\perp)n(E_\perp)\propto e^{-2}\eta^{-1}dJ_C/dV_{CB},$$

where $\eta=e^{-1}d\Phi_C/dV_{CB}$ is a proportionality factor. If

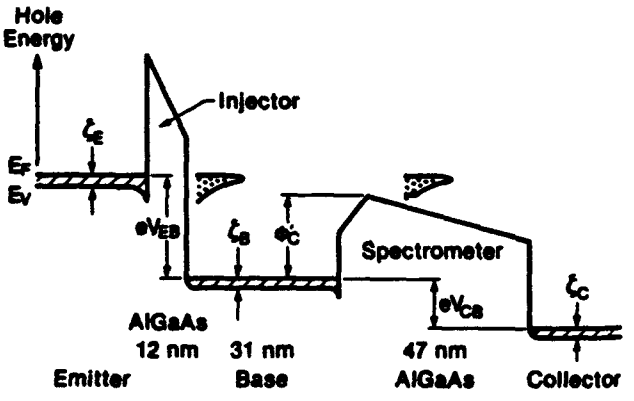

FIG. 1. Valence band in the hot-hole transistor with hole energy plotted upward. The tunnel injector and spectrometer barriers have AlAs mole fractions of 0.5 and 0.31, respectively. The collector is shown biased negatively. The emitter, base, and collector are p^+-GaAs doped to a level of 1.6×10^{18} cm^{-3}.

our graded barrier were ideal, for $V_{CB} > 0$ we would have $\eta \simeq 1$ (with peak potential at collector side), and for $V_{CB} < 0$, $\eta \simeq \frac{6}{47} = 0.13$ (with peak 6 nm away from the base side). However, some barrier parameters such as the density of any unintentional charges,[7] of the extent of acceptor (Be) segregation from the collector,[8] are important and difficult to determine accurately. Thus, a study of the spectrometer barrier, leading to the actual Φ_C and η, has to be done.

This study is done, with our hot-hole transistor structure, by our finding a low-temperature threshold injection voltage, V_{EB}^{*}, for some V_{CB}, for which an onset in the collector current occurs. Then the Fermi level in the emitter is at the same height as the peak potential of the collector barrier, and some ballistic holes can graze and pass the top of the barrier.[9] More accurately, the collector-barrier height is $\Phi_C = eV_{EB}^{*} + \zeta_B + \delta$, where ζ_B is the Fermi energy in the base (Fig. 1), and $\delta \simeq 10$–20 meV is a correction due to holes tunneling somewhat below the barrier top. The results of such experiments, done at high current sensitivities, are seen in Fig. 2(a). From here, with neglect of δ, the collector-barrier height above the Fermi level in the base, $\Phi_C' = eV_{EB}'$, is plotted in Fig. 2(b). With no bias applied $\Phi_C' = 170$ meV and $\zeta_B \simeq 9$ meV for our doping, and thus $\Phi_C = 179$ meV $+ \delta$, a value higher by at least 20 meV than the published band-discontinuity values.[10] This difference is most probably related to unintentional positive charges in the barrier, which we address below.

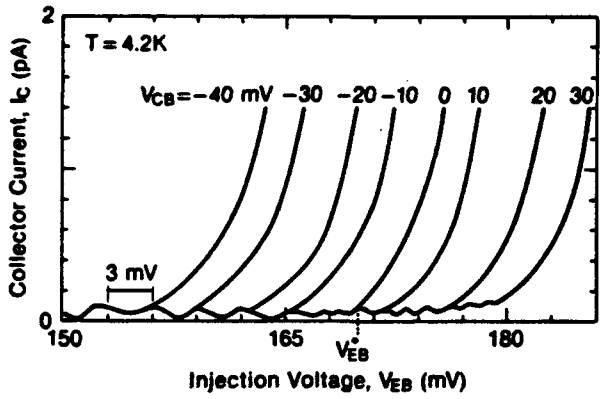

(a)

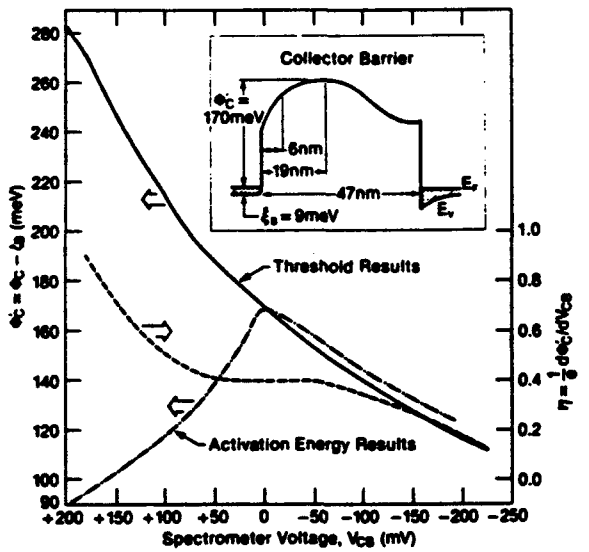

(b)

FIG. 2. (a) Collector-current onsets for different V_{CB}, and an example of determining the threshold eV_{EB}^{*} for $V_{CB} = 0$. Note the very small currents rising from the noise line. (b) Φ_C' and the derivative η as functions of V_{CB}. Also plotted are the barrier heights from separate measurements of activation energy for thermionic emission [for $V_{CB} > 0$ (< 0) the barrier is that for holes in the collector (base)]. Inset: A probable collector-barrier shape.

Figure 2(b) also gives the calculated η, which together with Φ_C' is sufficient for the analysis of our spectroscopy experiments; however, the study of Φ_C and η in some detail gives us a physical insight of the barrier shape, as related to actual barrier parameters. In the range -50 mV $< V_{CB} < 50$ mV, $\eta = 0.4$, suggesting a barrier peak at some 0.4×47 nm $= 19$ nm away from the base side. This, and the increase in the barrier height from the value given in Ref. 10 (seen above), can result from unintentional positive charges in the barrier, charges which we independently measured.[11] One can also see that η approaches unity only at large positive V_{CB}, an effect that can be attributed to barrier lowering on the collector side, most probably due to Be segregation into the barrier during growth.[8] This was verified by measurement of activation energies for thermionic emission, with results given in Fig. 2(b).[10] The method proved credible as seen from the good agreement between the activation energy results for $V_{CB} \leq 0$, and Φ_C' determined from the threshold measurements. For large positive V_{CB} we find a rather low barrier height on the collector side, $\Phi_C - \zeta_C \simeq 90$ meV. From these results a more realistic shape of the collector barrier is shown in the inset in Fig. 2(b). This barrier has a potential peak that moves from near the base side to the collector side as V_{CB} increases.

Spectroscopy was done by the measurement, at 4.2 K, of the collector current I_C versus the collector voltage V_{CB}, at different injection voltages V_{EB} [Fig. 3(a)]. The current rises steeply up to a knee where the slope clearly changes. The hole energy distributions, shown in Fig. 3(b), are derived by the division of the dI_C/dV_{CB} curves by the η determined above, and the conversion of the horizontal scale to excess normal energy above ζ_B [with use of Fig. 2(b)]. A few interesting features can be noticed. For injection energies in the range 190–210 meV, a clear ballistic behavior is observed. The distributions are extremely sharp with widths at half maximum of $\simeq 35$ meV, and peaks tracking exactly the injection energy, eV_{EB} (10 meV apart). At the lower-energy end, decaying tails of distributions, peaking somewhere closer to

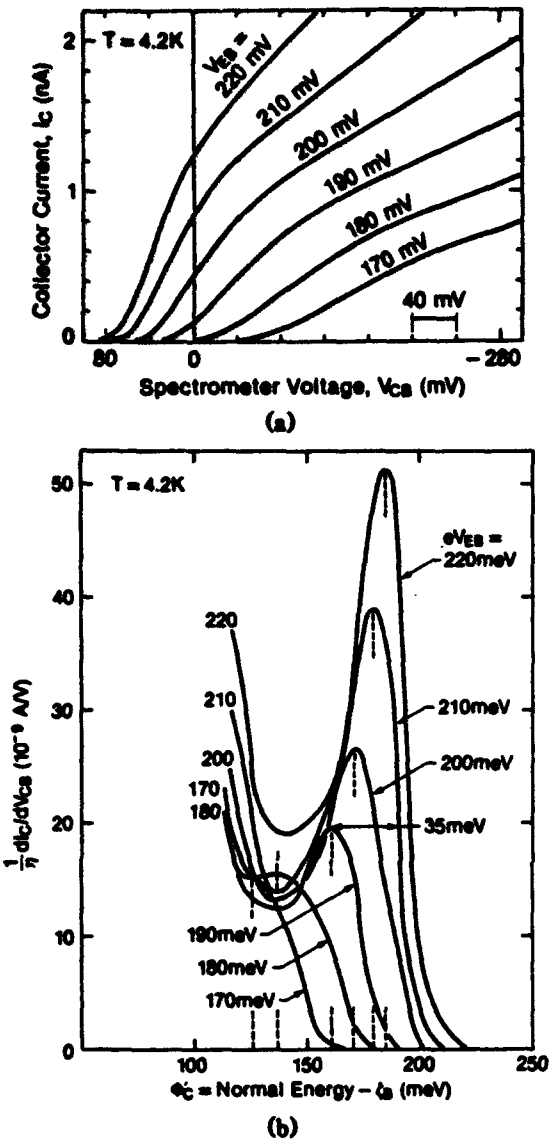

FIG. 3. (a) Collector current I_C vs spectrometer voltage V_{CB}, for different injection voltages V_{EB}. (b) Hole energy distributions deduced from the above $I_C - V_{CB}$ curves and the η given in Fig. 2(b). Ballistic peaks are seen for V_{EB} = 190, 200, and 210 mV. For lower V_{EB}, upper energy tails of nonballistic hole distributions are dominant.

the base Fermi level, are seen, masking the corresponding lower energy ballistic peaks. These tails are likely to originate from holes excited up from the equilibrium hole population in the base.[12] For $eV_{EB} > 220$ meV, peaks do not shift in energy any more, as the spectrometer potential peak moves rapidly toward the collector side. Then holes, most probably, cannot traverse ballistically the full width of the AlGaAs barrier against a relatively strong retarding electric field, resulting in a drop of the collector current and in an artificial peak in dI_C/dV_{CB}.

The observed hole distributions are narrower by a factor of 2 compared with those of ballistic electrons measured by a similar technique.[4] This is due to the narrower supply function in the emitter being determined by the heavy holes: ζ_E + band bending (calculated classically) ≃ 27 meV for V_{EB} = 200 mV. The small displacement in the peak positions below the Fermi level in the emitter is fully accounted for when we note that the injected distribution $n(E_\perp) \sim (E_F - E_\perp) D(E_\perp)$ at 0 K, where $D(E_\perp)$ is the one-dimensional tunneling probability, peaks some 15 meV below E_F,[4,13] and that the actual Φ'_C is higher by δ than the one used in Fig. 3(b). The above results are consistent with ballistic transport of the narrow distributions. Integrating the area under the distributions, we find that 8%–11% of the injected hole current is ballistic, with a calculated mfp ≃ 14 nm [by use of 0.1 = exp(−31/mfp)].

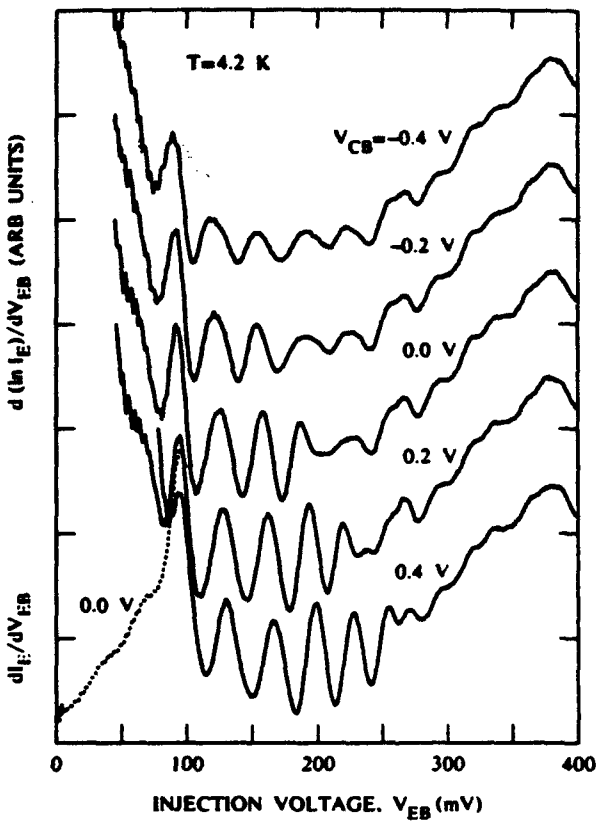

FIG. 4. Solid curves are the derivative of the logarithm of the injected current (high-frequency oscillations at the low V_{EB} are due to noise). As the collector voltages changes from positive to negative, fewer bound states are visible. The dotted line is dI_E/dV_{EB} for V_{CB} = 0, showing the lower-energy resonances.

Even though it is highly likely that the observed ballistic holes are light, the spectroscopy measurements described above are not sufficient to prove it. Confirmation is provided by the analysis of strong resonances resulting from hole interference effects, observed in the injection tunneling currents, at certain energies that are particularly sensitive to the effective mass of the holes.[6] These resonances are due to a faster increase in the injection current whenever the Fermi level in the emitter crosses

the bottom of a quasi-2D hole band formed in the base. Figure 4 shows the derivatives $d(\ln I_E)/dV_{EB} - V_{EB}$, for different V_{CB}. As long as $eV_{EB} \leq \Phi_C'$, strong oscillations in the derivative are observed because the participating 2D states are strongly bound. However, when $eV_{EB} > \Phi_C'$, the oscillations are due to the less confined (virtual) states, and thus weaker. As seen in Fig. 4, when the collector voltage changes from positive (high Φ_C) to negative (low Φ_C) values, the topmost bound states gradually become virtual, and the corresponding oscillations get weaker.[6] The observation of the peaks due to interference effects confirm the ballistic transport of the holes.

In order to find the corresponding ballistic-hole mass, we have estimated the positions of the bound light-hole states in a symmetric square well, 31 nm wide and 200 meV deep. Obviously this is a gross simplification since it ignores the exact potential distribution in the base and the nonparabolicity effects of the hole band; however, it distinctly shows the nature of the ballistic holes. For $m_{lh} = 0.082 m_e$, we find bound levels at 3, 15, 35, 62, 97, 138, and 182 meV.[14] From Fig. 4, for $V_{CB} = 0$, the observed bound peak positions including ζ_B are at 41, 72, 102, 133, and 168 meV, agreeing well with the calculations (the first two calculated levels are not seen since they are just at or below the Fermi level). Note that at energies higher than 100 meV the well widens and nonparabolicity increases the light-hole effective mass,[5] causing the last two observed peaks to be at somewhat lower energies. For comparison, heavy holes with $m_{hh} = 0.51 m_e$ would have sixteen bound states in the base, excluding them from the observed transport.

In summary, our results show, for the first time, unambiguous spectroscopic observation of ballistic light-hole transport in GaAs. Ballistic hole distributions, 35 meV wide, with a mean free path of about 14 nm, have been measured. Lower energy distributions, that might be due to excited holes from the Fermi bath, are observed too. Quantum interference effects in the thin transport regions provide added evidence for the ballistic transport.

We thank L. F. Alexander and C. Lanza for their technical help. We also thank E. E. Mendez and A. C. Warren for their help in some of the calculations, and J. Batey, M. V. Fischetti, A. B. Fowler, S. P. Keller, C. J. Kircher, and F. Stern for their comments on the manuscript. This work was partly supported by the U.S. Defense Advanced Research Projects Agency and administered by the U.S. Office of Naval Research Contract No. N00014-87-C-0709.

[1]R. J. von Gutfeld and A. H. Nethercot, Jr., Phys. Rev. Lett. 18, 855 (1967).

[2]L. F. Eastman, R. Stall, D. Woodard, N. Dandekar, C. E. C. Wood, M. Shur, and K. Board, Electron. Lett. 16, 525 (1980).

[3]R. Trzcinski, E. Gmelin, and H. J. Queisser, Phys. Rev. B 35, 6373 (1987).

[4]M. Heiblum, M. I. Nathan, D. C. Thomas, and C. M. Knoedler, Phys. Rev. Lett. 55, 2200 (1985); M. Heiblum, I. M. Anderson, and C. M. Knoedler, Appl. Phys. Lett. 49, 207 (1986).

[5]J. C. Blakemore, J. Appl. Phys. 53, R123 (1982).

[6]M. Heiblum, M. V. Fischetti, W. P. Dumke, D. J. Frank, I. M. Anderson, C. M. Knoedler, and L. Osterling, Phys. Rev. Lett. 58, 816 (1987).

[7]T. W. Hickmott, P. M. Solomon, R. Fischer, and H. Morkoç, J. Appl. Phys. 57, 2844 (1985).

[8]D. L. Miller and P. M. Asbeck, J. Appl. Phys. 57, 1816 (1985).

[9]We may assume that some ballistic holes, few as they may be, always exist in the structure. We later prove their existence and find their number from spectroscopy measurements.

[10]J. Batey and S. L. Wright, J. Appl. Phys. 59, 200 (1986). The valence-band discontinuity $\Delta E_V = 5.5x$, where x is the AlAs mole percentage. For our AlGaAs collector barrier, $x = 31\%$ and $\Delta E_V = 171$ meV.

[11]Capacitance measurements done on separate p^+-intrinsic AlGaAs-p^- structures show a voltage shift in the flat-band condition consistent with positive charges in the barrier in the low 10^{16}-cm^{-3} range.

[12]Similar low-energy electron distributions had been reported by A. F. J. Levi, J. R. Hayes, P. M. Platzman, and W. Wiegmann, Phys. Rev. Lett. 55, 2071 (1985).

[13]M. Heiblum, Solid-State Electron. 24, 343 (1981).

[14]For 31-nm base thickness, light- and heavy-band mixing at $k = 0$ is insignificant. See, for example, S. Brand and D. T. Hughes, Semicond. Sci. Technol. 2, 1607 (1987).

High-mobility inverted selectively doped heterojunctions

Hadas Shtrikman,[a] M. Heiblum, K. Seo, D. E. Galbi, and L. Osterling
IBM, Thomas J. Watson Research Center, Yorktown Heights, New York 10598

(Received 5 September 1987; accepted 14 December 1987)

We have used reflection high-energy electron diffraction (RHEED) to study the surface recovery of AlGaAs under different conditions. A modified process for growth interruptions was then introduced, where a GaAs monolayer was grown at each growth stop, and the arsenic flux was turned off during the low-temperature phase of growth interruptions. Selectively doped inverted heterojunctions were grown using the modified growth interruptions together with low-growth temperature (to avoid Si and impurity segregation). This combined process gave reproducible electron mobilities as high as 460 000 cm^2/V s with sheet carrier concentration of 2×10^{11} cm^{-2} at 4.2 K.

Much attention has been focused on investigating the differences between normal and inverted selectively doped GaAs–GaAlAs heterojunctions. In the normal structures the doped AlGaAs layer is grown on top of the undoped GaAs layer, and thus the two-dimensional electron gas (2-DEG) is formed at the top edge of the undoped GaAs layer. In the inverted structures the undoped GaAs layer is grown on top of the AlGaAs layer, so that the 2-DEG is formed in the GaAs right on top of the AlGaAs layer.

The inferior low-temperature electron mobilities of inverted structures, always below 100 000 $cm^2/V\,s$[1,2] (compared with values as high as 5×10^6 $cm^2/V\,s$[3] for the normal structures), were attributed to result from two main problems: dopant (usually Si) and impurity segregation from the AlGaAs into the GaAs–AlGaAs interface, and the GaAs–AlGaAs interface roughness. However, the inverted structures have advantages for some applications due to the easier formation of Ohmic contacts and the better electrical isolation of the 2-DEG from the substrate. The growth of high-quality inverted interfaces is especially important for achieving good quality quantum well and superlattice structures (as they are comprised of an equal number of normal and inverted interfaces).

Past attempts to solve this problem did not lead to reproducible results and were only marginally successful. Si segregation was reduced by using low-growth temperatures,[4,5] which in turn dictated the use of low-growth rates in order to maintain a good crystalline quality. An attempt to improve the interface smoothness was done by reducing the Al mole fraction.[5] The best reported mobilities for the inverted structure were achieved by introducing a short superlattice in the AlGaAs below the 2-DEG, which was believed to reduce impurity movement and improve the surface smoothness.[6] However, these results were never further confirmed.

The important role of including short superlattices and performing growth interruptions in obtaining high-quality epitaxial layers and smooth interfaces by molecular-beam epitaxy (MBE) has already been recognized.[7,8] It has been related both to surface smoothing processes[9] facilitated by the surface migration of the atoms and to impurities gettering at the interfaces.[10]

We have first tackled the problem of improving the quality of inverted heterojunctions by applying growth interruptions in order to improve the quality of the AlGaAs layers. Using reflection high-energy electron diffraction (RHEED) intensity measurements we have optimized the conditions for periodic interruptions during the growth of AlGaAs layers. We thus combined periodic growth interruptions with low-growth temperature in the doped AlGaAs region (to avoid Si segregation) to give, for the first time, a reproducible procedure for growing high-mobility selectively doped single inverted heterojunctions. Electron mobilities as high as 460 000 $cm^2/V\,s$ were measured at 4.2 K with electron concentration of 2×10^{11} cm^{-2}.

The layers were grown in RIBER 1000-1 system under arsenic stabilized conditions. The intensity of the specular reflection in the RHEED pattern of a (100)-$c(2\times4)$ As-stable reconstructed surface, with the beam in the (110) azimuth was monitored as a function of time at different roughening and recovery conditions. The intensity of the RHEED pattern was recorded in the conventional way using an optical fiber and an amplifying system.[9]

The RHEED intensity time evolution clearly shows that the smoothness recovery of GaAs layers is much faster and more complete than the recovery of AlGaAs surfaces. Moreover, a similar enhanced recovery can be seen when only 1 or

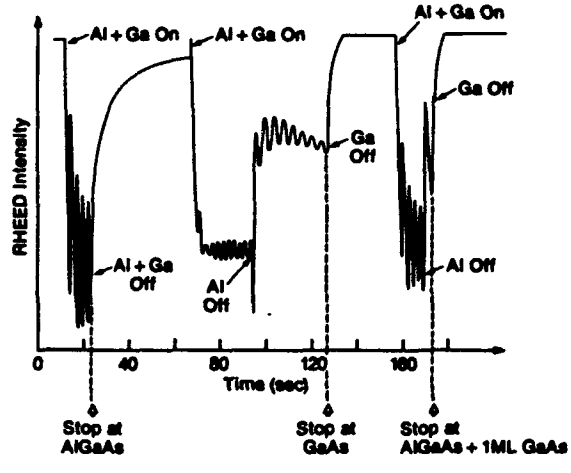

FIG. 1. A typical time evolution of RHEED specular beam intensity taken from (001)-2×4 reconstructed surface, during the growth and recovery of: (a) an AlGaAs layer (left-hand side), (b) 10 ML of AlGaAs covered by 8 ML of GaAs (center), and (c) a few AlGaAs monolayers covered by 1 ML of GaAs (right-hand side).

2 monolayers (ML) of GaAs are grown on top of an AlGaAs layer. A comparison between surface recoveries at various conditions is given in Fig. 1 for layers grown at 600 °C. The recovery of an $Al_{0.21}Ga_{0.79}As$ surface is seen at the left end of the figure. The following RHEED intensity oscillations reflect the growth of 10 AlGaAs ML followed by 8 GaAs ML. The GaAs surface recovery is considerably faster and more complete (the intensity goes out of scale). We concluded that even a deposition of a single GaAs monolayer on the AlGaAs surface is sufficient for enhancing the recovery process; as can be seen on the right-hand side of Fig. 1. The RHEED intensity recovery is as fast and complete as in the case of the thicker deposition of GaAs on top of AlGaAs.

The arsenic flux is normally left on during growth interruptions, while the substrate temperature is near the congruent sublimation temperature (~600 °C) or above it, in order to prevent the decomposition of the surface. However, we found that at substrate temperatures as low as 500 °C arsenic molecules impinging on the surface during growth stops lead to a roughening of the surface. Figure 2 shows the RHEED intensity from a GaAs surface maintained at 520 °C. The RHEED intensity decreased during growth interruption as long as the arsenic flux was impinging on the surface. As soon as the impinging arsenic flux was turned off the RHEED intensity increased significantly, reflecting the enhanced surface recovery.

Selectively doped inverted heterojunctions investigated in this work were basically conventional (in doping, mole fraction, and growth temperature) structures with a single 2-DEG located in the GaAs on top of the doped AlGaAs layer. A schematic description of the layers configuration is given in Fig. 3. A 0.5-μm-thick buffer layer was first grown at a growth rate of 0.7 μm/h at a substrate temperature of 600 °C. The growth rate was then reduced to 0.20 μm/h, in order to maintain a high-crystalline quality during the subsequent lower temperature growth of 500 °C using during the growth of the Si doped 10-nm-thick $Al_{0.21}Ga_{0.79}As$ layer. Two undoped $Al_{0.21}Ga_{0.79}As$ spacers were grown, the top one ranged from 4–25 nm and the bottom was 100 nm. The bottom spacer prevented a 2-DEG from forming at the bottom (normal) interface. Periodic growth interruptions (including a GaAs recovery monolayer) were introduced during the growth of the AlGaAs layers, according to the procedure described above. A 120-nm-undoped GaAs layer followed the top AlGaAs spacer, capped by 30-nm-thick Si doped GaAs that was designed to be fully depleted by the surface potential.

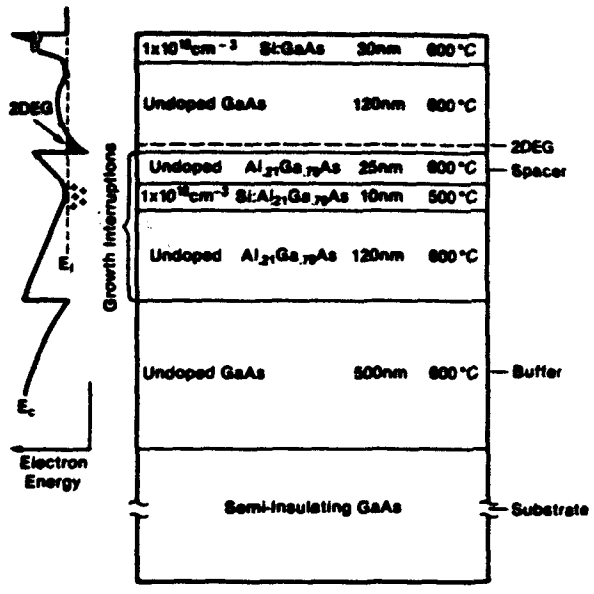

FIG. 3. A schematic cross-sectional view of a typical inverted selectively doped heterostructure, emphasizing the layers in which 20 s long growth interruptions were introduced. A schematic presentation of the respective conduction band diagram is given on the left-hand side of the figure.

Special care was taken to use more frequent growth interruptions at the top 5 nm of the AlGaAs spacer layer. There, we have used a growth stop every 5 ML of AlGaAs. Figure 4 shows the RHEED intensity oscillations recorded during

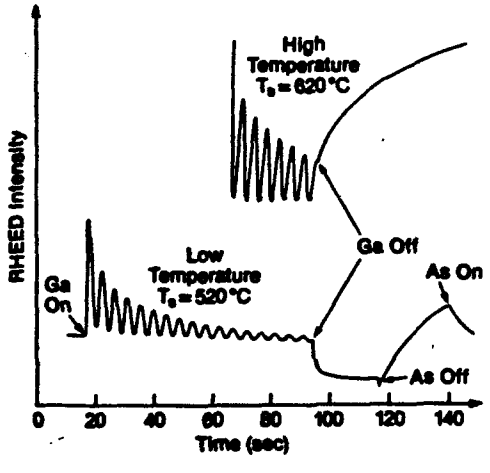

FIG. 2. A typical time evolution of RHEED specular beam intensity taken from (001)-2×4 reconstruction surface, during the growth and recovery of GaAs at 520 °C (bottom) and at 620 °C (top).

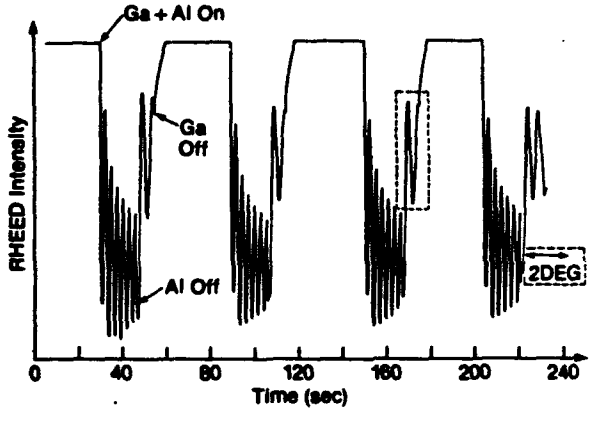

FIG. 4. The RHEED intensity time dependence taken during the growth of the top portion of the AlGaAs spacer layer. The GaAs stop layer can be clearly seen, after each interruption. One of the GaAs stop layers is indicated by a broken line, as well as the point at which the growth of the undoped GaAs layer begins (where the 2-DEG resides).

TABLE I. The mobilities and carrier concentrations of selectively doped inverted structures, measured at 300, 77, and 4.2 K.

	Spacer	300 K		77 K		4.2 K	
		μ $cm^2/V\,s$	n_s cm^{-2}	μ $cm^2/V\,s$	n_s cm^{-2}	μ $cm^2/V\,s$	n_s cm^{-2}
With many growth stops	25 nm	5000	7.5×10^{11}	130 000	2.5×10^{11}	460 000	2×10^{11}
With one growth stop	24 nm	5000	8×10^{11}	90 000	3×10^{11}	200 000	2.5×10^{11}
No growth stops	20 nm	6000	8×10^{11}	75 000	3.7×10^{11}	150 000	3.6×10^{11}

the growth of the top portion of the AlGaAs spacer. The GaAs recovery layer is clearly seen at each stop, as well as the point at which the growth of the undoped GaAs top layer was initiated. Note that no growth stop was introduced at the very top interface of the AlGaAs layer due to the fear of impurities incorporation at this critical growth interface.

Mobilities and sheet electron concentrations of some structures grown under different conditions that were measured at 300, 77, and 4.2 K in the dark are detailed in Table I. Mobilities as high as 460 000 $cm^2/V\,s$ with a sheet carrier concentration of 2×10^{11} cm^{-2} were measured at 4.2 K in structures which were grown with many growth interruptions. A lower but still comparatively high 4.2 K mobility of 200 000 $cm^2/V\,s$ are achieved for the growth in which only a single 1 min long, growth stop was introduced, some 3 nm below the AlGaAs–GaAs interface with no GaAs stop layer. These results are compared with the values achieved when no growth stops were used but the growth temperature was reduced during the growth of the Si-doped AlGaAs layer, to prevent the Si segregation and possible impurities migration. The electron mobility in this case was 150 000 $cm^2/V\,s$ at 4.2 K for a spacer thickness of 20 nm. We grew some structures with a 4-nm-thick AlGaAs top spacer, using one growth stop 30 nm below the AlGaAs–GaAs interface. The 77 K electron mobility in this case was 70 000 $cm^2/V\,s$ with a sheet carrier concentration of 8×10^{11} cm^{-2}.

We found that low-temperature growth was needed in order to prevent Si segregation or impurities propagation to the top interfaces. The latter was further demonstrated by growing "normally-off" structures. In these structures, grown on conductive substrates, AlGaAs is undoped and the 2-DEG is accumulated by the application of a positive voltage on the substrate with respect to the top contacts. In these structures, even though Si was not present, it was still essential to reduce the growth temperature within the later part of the AlGaAs layer growth, in order to achieve a high mobility. This clearly indicates that unintentional impurities are present and migrate at higher temperatures towards the top interface. Resuts on the normally-off inverted devices will be published elsewhere.[11]

We relate the enhanced surface recovery of the GaAs covered AlGaAs surfaces to the higher surface diffusion of Ga atoms on GaAs compared with Al and Ga atoms on AlGaAs. The activation energies, for diffusion E_D, were found to be 1.3 and 1.6 eV for Ga on GaAs and Al on AlGaAs, respectively.[12] As a result, the average terrace width on AlGaAs is significantly smaller than on GaAs, reflecting the faster recovery of a GaAs surface. Furthermore, shutting down the arsenic flux during the low temperature (500 °C) growth stops reduces the relative amount of GaAs molecules on the surface which in turn enables the Ga atoms to diffuse much faster.[13] Another mechanism which could be responsible for the improvement in the electron mobilities could be the trapping of impurities at each of the interfaces formed during the growth interruptions layers.[10]

In conclusion, we present for the first time, a reproducible procedure for growing high-mobility selectively doped inverted heterojunctions. The key features are the low-growth temperature to avoid Si and impurities segregation, the slow growth rate and the introduction of modified periodic growth interruptions during the growth of the AlGaAs layers. Mobilities as high as 460 000 $cm^2/V\,s$ and sheet carrier concentration of 2×10^{11} cm^{-2} were measured at 4.2 K in the dark.

Acknowledgments: The authors would like to thank U. Meirav for fruitful discussions. The project was supported partly by DARPA and administered by the Office of Naval Research Contract No. N00014-87-C-0709.

[a] Permanently at Soreq Nuclear Research Center, Yavne 70600, Israel.

[1] H. Morkoç, T. J. Durmmond, R. E. Thorne, and W. Kopp, Jpn. J. Appl. Phys. 20, L913 (1981).
[2] S. Sasa, J. Saito, S. Nanbu, T. Ishikawa, and S. Hiyamizu, Jpn. J. Appl. Phys. 23, L573 (1984).
[3] J. H. English, A. C. Gossard, H. L. Störmer, and K. W. Balkwin, Appl. Phys. Lett. 50, 1826 (1987).
[4] K. Inoue and H. Sakaki, Jpn. J. Appl. Phys. 23, L61 (1984).
[5] M. Heiblum, J. Vac. Sci. Technol. B 3, 820 (1985).
[6] T. J. Drummond, J. Klem, D. Arnold, R. Fisher, R. E. Thorne, W. G. Lyons, and H. Morkoç, Appl. Phys. Lett. 42, 615 (1983).
[7] H. Sakaki, M. Tanaka, and J. Yoshino, Jpn. J. Appl. Phys. 24, L417 (1985).

[8]S. Clarke and D. D. Vvedensky, Appl. Phys. Lett. 51, 340 (1987).
[9]J. M. Van Hove, C. S. Lent, P. R. Pukite, and P. I. Cohen, J. Vac. Sci. Technol. B 1, 741 (1983).
[10]P. M. Petroff, R. C. Miller, A. C. Gossard, and W. Wiegmann, Appl. Phys. Lett. 44, 217 (1984).
[11]U. Meirav, M. Heiblum, and F. Stern, Appl. Phys. Lett. (in press).
[12]B. A. Joyce, in Proceedings of the 2nd International Conference on Modulated Semiconductor Structures, Kyoto (1985), p. 1.
[13]Y. Horikoshi, M. Kawashima, and H. Yamaguchi, Jpn. J. Appl. Phys. 25, L868 (1986).

High-mobility variable-density two-dimensional electron gas in inverted GaAs-AlGaAs heterojunctions

U. Meirav
Department of Physics, Massachusetts Institute of Technology, Cambridge, Massachusetts 02139
M. Heiblum and Frank Stern
IBM T. J. Watson Research Center, Yorktown Heights, New York 10598

(Received 2 February 1988; accepted for publication 16 February 1988)

Inverted heterointerfaces (GaAs on AlGaAs), which are basic constituents of all quantum wells and superlattices, have been significantly improved using electron diffraction and a refined molecular beam epitaxy growth procedure. Utilizing them in a novel structure allowed the variation of the electron density over a wide range, with peak mobilities of 4×10^5 cm^2/V s. The continuously variable electron density allowed comparison to a theoretical analysis of the low-temperature scattering mechanisms, and their relation to the growth process, establishing the importance of interface charges and roughness. High-mobility samples were used to observe the quantum Hall effect with varying carrier concentrations in a single structure.

A high-mobility quasi-two-dimensional electron gas (2DEG) can now be routinely produced in GaAs-AlGaAs normal heterojunctions where a doped AlGaAs alloy is grown on top of a pure GaAs layer.[1] So far, in the inverted heterojunctions, where the pure GaAs is grown on top of the AlGaAs, 2DEG mobilities were relatively low. Inverted heterojunctions are extremely important since half of the interfaces in GaAs-AlGaAs quantum wells and superlattices are inverted. Single inverted interfaces also have some technological advantages.[2] Attempts to improve inverted structures have been reported before,[3-5] but the difficulties were never resolved. Two main reasons were offered to explain the low mobilities in the inverted structures: (a) interface roughness that is inherent to the growth process, and (b) impurity segregation during growth towards the interface and the top GaAs layer.

We report here a study that led to the development, for the first time, of high-mobility inverted interfaces. Moreover, the interface was embedded in a novel structure (an inverted semiconductor-insulator-semiconductor, or ISIS) that enabled the variation of the 2DEG density continuously from the low value of 2×10^{10} to 5×10^{11} cm^{-2} in a single structure, with mobilities approaching those measured in normal heterojunctions. We find strong correlations between the electron mobility and the AlGaAs interface smoothness, as indicated by the intensity of grazing angle reflection high-energy electron diffraction (RHEED) spots.

A variable density 2DEG formed at an interface could facilitate its study, and in particular be useful for inverted structures. Hence, a novel ISIS structure was developed where the 2DEG is formed by the application of an electric field at the GaAs-AlGaAs inverted interface. The structure, grown by molecular beam epitaxy (MBE), is described in Fig. 1. Mesas $\simeq0.2$ μm deep were etched, and four (or six) lithographically defined AuGe/Nb/Au shallow ohmic contacts were alloyed (to a depth of $\simeq150$ nm, avoiding shorting to the gate) to form a Van der Pauw (or a Hall bar) pattern. Initially no 2DEG is formed, and current does not flow between the top contacts. As the (positive) gate voltage is increased above a threshold voltage of $\simeq1$ V, the sheet density n_s of the 2DEG increases proportionally to the electric field at the interface (see Fig. 1).

Our initial attempts to produce inverted structures resulted in a relatively low 4.2 K mobility of 5×10^4 cm^2/V s, as also obtained by other researchers.[4,5] However, normal structures with donors in the AlGaAs and thick AlGaAs spacer layers, grown under the same conditions, had mobilities of some 4×10^5 cm^2/V s. In order to overcome these fundamental differences, which are obviously interface related, we have exploited the RHEED technique,[6] observing the specular reflection pattern of an electron beam in the (110) direction during growth. The diffraction intensity, corresponding to the surface smoothness,[6] exhibits decaying oscillations as GaAs growth proceeds. Each oscillation corresponds to a single monolayer growth time, due to a periodic roughening and smoothing of the surface. The overall decay results from the increased roughness with increasing

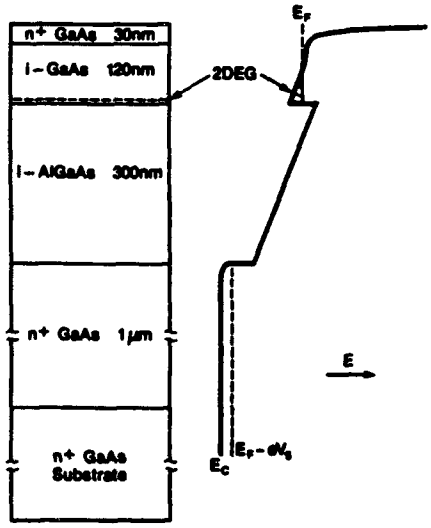

FIG. 1. Description of an ISIS structure. The potential diagram on the right corresponds to the accumulation mode. The top doped GaAs layer is designed to be exactly depleted by the surface potential.

 0003-6951/88/151268-03$01.00

layer thickness. When growth is interrupted, the smoothness of the surface improves and RHEED intensity increases over a time period determined by the growth conditions. When AlGaAs is grown, surface roughness builds up more rapidly than in the GaAs case, and the recovery is much slower and incomplete. This is due to the low surface mobility of the Al atoms, responsible for the greater roughness of the inverted interface.[7,8]

In order to smooth the top AlGaAs surface the growth was interrupted frequently under excess As flux,[9] and its rate reduced to 4 nm per minute, to allow the Al atoms reach terrace steps and nucleate smoothly.[7] The resultant electron mobility was thus improved, and reached a peak value of 10^5 cm^2/V s for a density $n_s \simeq 6\times10^{11}$ cm^{-2}. However, the mobility dropped very sharply (to a few thousands) when n_s was reduced to 2×10^{11} cm^{-2}.

A deposition of about one monolayer (1 ML) of GaAs on the AlGaAs surface just before growth interruption led to substantially faster and more complete smoothness recovery. Figure 2 compares RHEED intensity oscillations during AlGaAs growth followed by the recovery of both AlGaAs and AlGaAs + 1 ML of GaAs. The shorter interruption time is highly advantageous since the number of incorporated impurities from the surrounding is minimized. Employing this technique in the growth of the AlGaAs ($x\simeq0.26$) improved the peak mobility to 1.5×10^5 cm^2/V s. The mobilities and sheet densities, shown in the lower part in Fig. 3, were measured by the Van der Pauw method, while varying the gate voltage V_g. The maximum achievable n_s was limited by the onset of leakage current into the gate due to tunneling through the resulting triangular potential barrier of the AlGaAs.

A further and crucial step involved the reduction of impurity movement toward the interface. This was accomplished by reducing the substrate temperature to 500 °C during the growth of a thin AlGaAs layer some 5 nm below the inverted interface (thereafter the temperature was quickly raised). This procedure, in conjunction with reducing the AlAs mole fraction to 0.21, produced superior inverted structures with an extremely wide range of electron densities, from n_s as low as 2×10^{10} cm^{-2} up to 5×10^{11} cm^{-2}, and a maximum mobility of 4×10^5 cm^2/V s (upper curve of Fig. 3).[10] The mobility increases sharply as the electron density increases and then levels off. Good ohmic contacts to the 2DEG were maintained even at the extremely low density range.

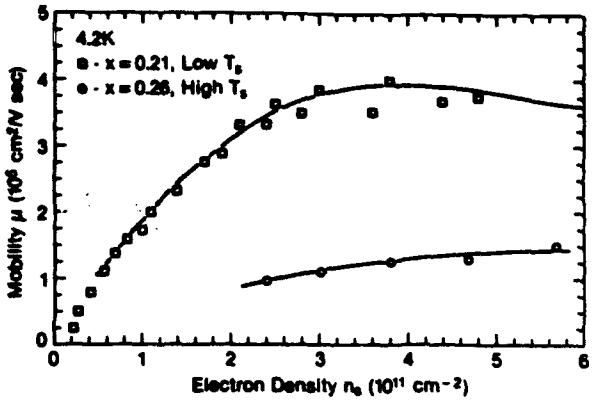

FIG. 3. Mobility vs 2DEG density (controlled by a gate voltage) in two ISIS structures. The results at the bottom (circles) are for an inverted interface with AlAs mole fraction $x\simeq0.26$ grown at a high substrate temperature, thus suffering from high interface charge density and more roughness. The top results (squares) are for $x\simeq0.21$ incorporating a thin AlGaAs region grown at a low temperature. The lines are calculation results from a simple model invoking roughness, interface charges, and bulk impurities.

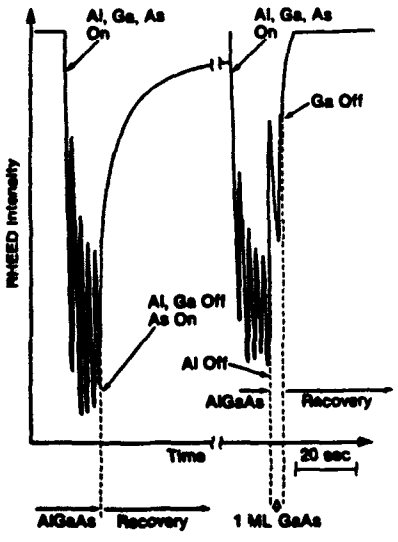

FIG. 2. Description of RHEED intensity oscillations during GaAs and AlGaAs growth followed by surface smoothness recovery facilitated by growth interruption. At left, a relatively long recovery time is required for a bare AlGaAs surface. At right, the faster and more complete recovery of the same AlGaAs surface covered by a monolayer of GaAs (intensity is saturated).

To understand this dependence and to analyze electron scattering in these inverted structures, we applied an approximate model[11] that includes scattering by background impurities in the GaAs, by interface charges at the GaAs-AlGaAs interface, and by interface roughness. A Fang–Howard envelope wave function (i.e., infinite barrier height approximation) was used, and the calculation made an approximation for the effective depletion field, that does not accurately reflect the more complicated potential profile near the interface (due to the vicinity of the GaAs-vacuum interface). The calculation was otherwise conventional.[12] The interface roughness was characterized by a Gaussian autocorrelation function with rms step height $\Delta = 0.2$ nm corresponding to one monolayer steps (somewhat smaller than the value used by Hirakawa *et al.*[13] in thin quantum wells) and a lateral correlation length $\Lambda = 5.5$ nm. It was necessary to invoke a density of 5×10^9 cm^{-2} interface charges to account for the low mobility at low electron densities. The background acceptor concentration was taken to be 7×10^{14} cm^{-3}, approximately consistent with values found for other samples grown under similar conditions. As shown in Fig. 3, an excellent fit was achieved over the entire range of electron densities for this higher mobility sample (with $x\simeq0.21$). The data measured on the lower quality sample ($x\simeq0.26$) could be accounted for by a rougher interface with about 3×10^{10} cm^{-2} interface charges. While no great significance should be attached to the specific numerical val-

ues used in the analysis, it seems clear that both interface charges and interface roughness are required to explain our results. Furthermore, the changes in these quantities resulting from different growth procedures give a direct qualitative correlation between RHEED intensity and interface roughness and also between the growth temperature and the accumulation of charged impurities at the interface, as reflected by Coulombic scattering.

Since a 2DEG in inverted structures has never been shown to exhibit the quantum Hall effect before, low-temperature (0.5 K), high magnetic field (15 T) measurements were carried out on these structures with Hall bar geometries. The potential of this inverted structure is demonstrated by doing the measurements at different gate voltages thus varying the density over a wide range. We have observed the quantized Hall effect, including magnetoresistance dips at some fractional filling factors as shown in Fig. 4(a). The shift in the positions of the minima in R_{xx} at different carrier densities is clearly demonstrated. Figure 4(b) gives R_{xx} and R_{xy} as a function of the gate voltage (and consequently the carrier density) at 3 T.

In summary, we report the study of inverted heterojunctions with a two-dimensional electron gas (2DEG). We have shown that charges and roughness at the interface are responsible for the generally poor quality of inverted structures. The growth process has been refined with the use of high-energy electron diffraction, leading to peak mobilities at 4.2 K of 4×10^5 cm^2/V s. Moreover, this interface was incorporated in a novel structure (ISIS) which allowed us to vary the electron density continuously, over a wide range, by the application of a gate voltage. A numerical calculation using a simple model allowed the determination of the dominant scattering mechanisms influencing the mobility of the 2DEG, which were clearly related to the different growth procedures. We have demonstrated how the structure could be exploited by measuring the quantum Hall effect over a wide range of carrier densities and mobilities.

Note added in proof. A similar ISIS structure for charged injection purposes was worked on before by A. Kastalsky, J. H. Abeles, R. Bhat, W. K. Chan, and M. A. Koza [Appl. Phys. Lett. 48, 71 (1986)].

We would like to thank H. Shtrikman and L. Osterling for help with RHEED analysis and MBE growth, D. Face for participating in Hall measurements, M. A. Kastner, H. I. Smith, D. A. Antoniadis, and A. C. Warren for useful discussions, and J. Carter, B. Brandt, and M. S. Christie for technical assistance. Hall measurements were done in the Francis Bitter National Magnet Laboratory. The work at IBM was partly supported by Defense Advanced Research Projects Agency and administered by Office of Naval Research, contract No. N00014-87-C-0709. The work at MIT was supported by National Science Foundation grant ECS-8503443.

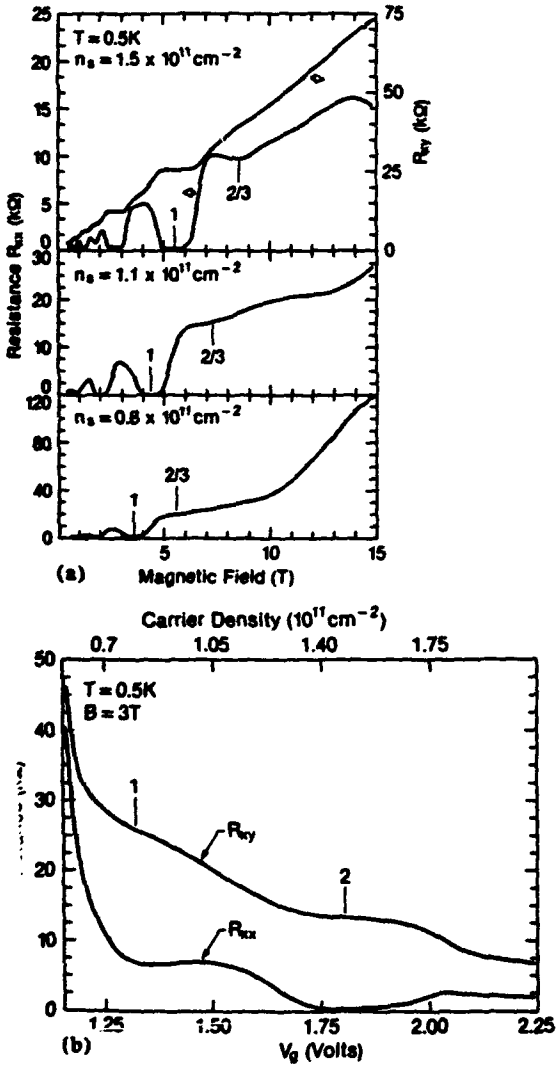

G. 4. Quantum Hall effect and magnetoresistance of the 2DEG at the erted interface. (a) The magnetoresistance as a function of magnetic d for three different gate voltages and 2DEG densities in a single struce. (b) The Hall resistance and the magnetoresistance at 3 T as a function gate voltage.

[1]L. C. Witkowsky, T. J. Drummond, C. M. S. Stanchak, and H. Morkoç, Appl. Phys. Lett. 37, 1033 (1980).
[2]The AlGaAs barrier isolates the 2DEG from the lower quality substrate, and ohmic contacts to the 2DEG are more easily formed.
[3]T. J. Drummond, J. Klem, A. Arnold, R. Fischer, R. E. Thorne, W. G. Lyons, and H. Morkoç, Appl. Phys. Lett. 42, 613 (1983).
[4]K. Inoue and H. Sakaki, Jpn. J. Appl. Phys. 23, L61 (1984).
[5]M. Heiblum, J. Vac. Sci. Technol. B 3, 820 (1985).
[6]J. M. Van Hove, C. S. Lent, P. R. Pukite, and P. I. Cohen, J. Vac. Sci. Technol. B 1, 741 (1983).
[7]M. Heiblum, E. E. Mendez, and L. Osterling, J. Appl. Phys. 54, 6982 (1983).
[8]B. A. Joyce, *Proceedings of the 2nd International Conference on Modulated Semiconductor Structures, Kyoto* (North-Holland, Amsterdam, 1985), p. 1.
[9]Each interruption lasted for about 1 min, with the last one some 4 nm below the inverted interface. An interruption at the inverted interface led to a decrease in the mobility, most probably due to impurity trapping.
[10]Employing the same procedure with inverted structures with intentional doping and 20 nm spacer layers in the AlGaAs, produced 2DEG with mobilities of 4.6×10^5 cm^2/V s. See H. Shtrikman, M. Heiblum, K. Seo, D. E. Galbi, and L. Osterling, J. Vac. Sci. Technol. B April/May (1988).
[11]F. Stern, Appl. Phys. Lett. 43, 974 (1983).
[12]T. Ando, A. B. Fowler, and F. Stern, Rev. Mod. Phys. 54, 437 (1982).
[13]H. Sakaki, T. Noda, K. Hirakawa, M. Tanaka, and T. Matsusue, Appl. Phys. Lett. 51, 1934 (1987).

Pseudomorphic InGaAs base ballistic hot-electron device

K. Seo, M. Heiblum, and C. M. Knoedler
IBM Research Division, T. J. Watson Research Center, Yorktown Heights, New York 10598

W-P. Hong and P. Bhattacharya
Department of Electrical Engineering and Computer Science, University of Michigan, Ann Arbor, Michigan 48109

(Received 25 May 1988; accepted for publication 8 September 1988)

We report the first successful incorporation of a pseudomorphic InGaAs base in a ballistic hot-electron device. The device, with a 28-nm-thick $In_{0.15}Ga_{0.85}As$ base, had a collector-base breakdown voltage of 0.55 V and a maximum current transfer ratio of 0.89 at 4.2 K, considerably higher than the 0.75 in a comparable GaAs-base device. Electron energy spectroscopy measurements revealed that at least 30% of the injected electrons traversed the InGaAs base ballistically, causing a strong modulation in the injected currents into the quantized base. The Γ-L valley separation in the strained $In_{0.15}Ga_{0.85}As$ was estimated to be about 410 meV.

We have recently reported on the dc performance of GaAs tunneling hot-electron transfer amplifier (THETA) devices and the direct evidence of ballistic electron transport through thin n^+-GaAs layers.[1,2] In a typical THETA device with a 30-nm-wide n^+-GaAs base doped to $\sim 1\times10^{18}$ cm^{-3}, about 30% of the injected current was observed to traverse the base ballistically, while the maximum differential current transfer ratio (α_M) was 0.75 at low temperatures.[2] By reducing the collector barrier height and thus increasing the available window for ballistic transport an $\alpha_M = 0.9$ was achieved.[1] However, the small collector barrier height limited the maximum allowed collector-base voltage without collector leakage to less than 0.3 V.

In this letter, we report the first successful incorporation of a 28-nm-wide n^+-$In_yGa_{1-y}As$ ($y = 0.15$) pseudomorphic layer as the base in the THETA device. This device is expected to suffer less from transfer to the L valleys due to a larger Γ-L valley separation. At the same time, the increased conduction-band discontinuity between AlGaAs and InGaAs enables us to reduce the AlAs mole fraction in the collector barrier for the same collector-base breakdown voltage. This tends to improve the quality of the AlGaAs and reduce the scattering of hot electrons in the collector barrier. Indeed we have found in the novel device a collector-base breakdown voltage of 0.55 V for an AlAs mole fraction of 0.15, and a maximum differential current transfer ratio $\alpha_M \simeq 0.89$ at 4.2 K.

The InGaAs pseudomorphic structures were grown by molecular beam epitaxy (MBE) on (100) n^+-GaAs substrates. Figure 1 describes the energy-band diagram of the device under normal bias conditions in a common-base configuration (CBC). The tunnel injector on the left is formed from a thin $Al_xGa_{1-x}As$ layer (10 nm, undoped, $x = 0.28$) which is sandwiched between an n^+-GaAs emitter and a 28-nm-thick n^+-$In_yGa_{1-y}As$ ($y = 0.15$) base which is doped to 1.1×10^{18} cm^{-3}. Another undoped $Al_xGa_{1-x}As$ layer (70 nm, $x = 0.15$) between the base and the n^+-GaAs collector layer forms the collector barrier, thus preventing the equilibrium electrons in the base from entering the collector. The AlAs mole fraction in the collector barrier is graded down to $x = 0.07$ over the last 10 nm on the base side to reduce the quantum mechanical reflections of the incoming hot electrons.

The measured output characteristics, I_C-V_{CB}, in a CBC at 4.2 K are shown in Fig. 2(a). These characteristics are very similar to those of a bipolar transistor. Due to the larger conduction-band discontinuity, the collector-base breakdown voltage (V_{CBM}) is about 0.55 V compared to $V_{CBM} \simeq 0.3$ V in the GaAs device with similar AlAs mole fraction in the collector barrier. The differential current transfer ratio-injection voltage characteristics, $dI_C/dI_E - V_{BE}$, of the same device are shown in Fig. 2(b). Note that the device has $\alpha_M \sim 0.89$ (0.87 at 77 K) that is substantially higher than $\alpha_M \sim 0.75$ in the GaAs devices with similar base doping and thickness.[2] Note also the resonances evident in the curves which are related to quantum mechanical interference of the ballistic electrons in the thin base and will be discussed later. We attribute the higher α_M to the larger Γ-L energy separation $E_{\Gamma L}$ in the strained InGaAs base.

When the injection energy is high enough, some of the ballistic electrons transfer to the L valleys in the base, resulting in a decrease in the current gain α. This was seen before in the GaAs THETA devices.[3] In the pseudomorphic InGaAs-base device, only a slight decrease in α is observed at high injection energies [Fig. 2(b)]. The value for $E_{\Gamma L}$ is

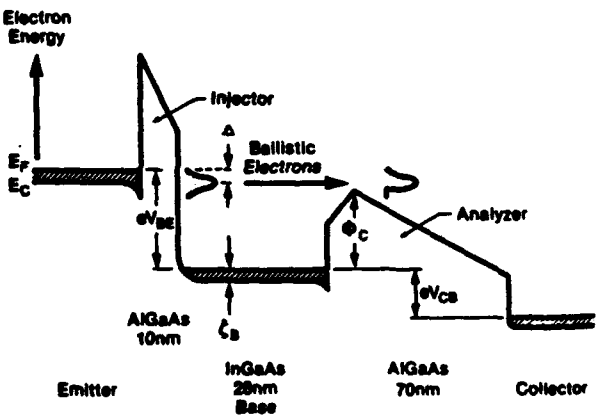

FIG. 1. Schematic diagram of the conduction band of a THETA device under forward bias operation.

 0003-6951/88/461946-03$01.00

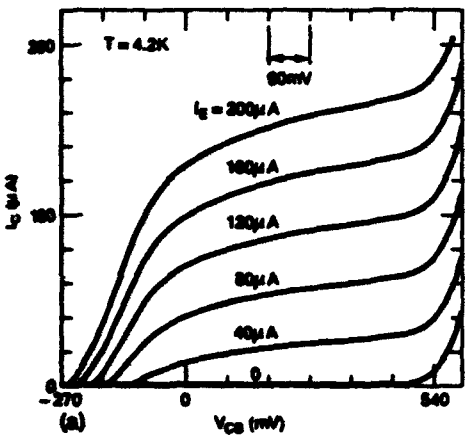

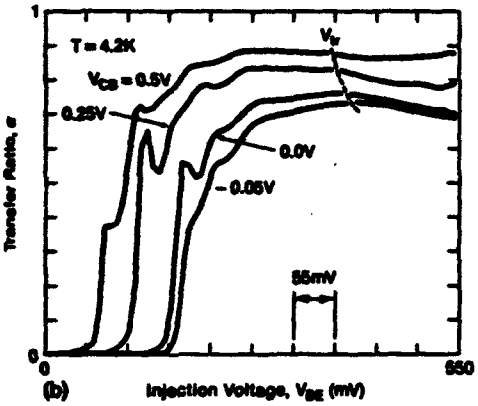

FIG. 2. Output current-voltage characteristics of the device at 4.2 K. The parameter is the injection current I_E. (b) The differential current gain α vs the injection voltage V_{BE} at 4.2 K. V_{tr} is the threshold voltage for the L-valley transfer.

the strained base can be estimated from the value of $V_{BE} = V_{tr}$ where α starts decreasing. If this point is associated with the Fermi level in the emitter being one phonon energy above the bottom of the L band, then

$$E_{\Gamma L} \sim qV_{tr} + \zeta_B - E_{ph} - qV_{BB},$$

where ζ_B is the Fermi energy in the base, E_{ph} the optical phonon energy at the edge of the Brillouin zone, and V_{BB} the voltage drop due to the parasitic base resistance. We estimate a Γ-L valley separation of about 410 meV (compared to 290 meV in GaAs[3]). This is somewhat bigger than ~370 meV predicted by the virtual crystal approximation.

Employing the "electron energy spectroscopy" technique,[1] the application of V_{CB} causes the potential height of the collector barrier above the Fermi level in the base, Φ_C, to change, thus affecting the collector current density J_C. The energy distribution associated with the perpendicular momentum (normal energy distribution) can be approximated by $(1/q\eta)(dJ_C/dV_{CB})$, where $\eta = (1/q)(d\Phi_C/dV_{CB})$ is a proportionality factor.[1] Since the potential shape of the collector barrier is complicated by barrier parameters that are difficult to control (unintentional charges,[4] Si segregation,[5] and the shape of the composition grading), the barrier height as a function of V_{CB} was determined from the activation energy for thermionic emission. In the temperature range 100 K $< T <$ 180 K, the linearities of $\ln(J_C/T^2)$ vs $(1/T)$ plots were good and the effective Richardson constant A was 0.8–1.2. The results in Fig. 3 show a linear dependence of the collector barrier height, Φ_C, on V_{CB} in the range greater than 40 mV. Since $\eta = 0.23$ in the range of our spectroscopy measurements (ideally it should be 10 nm/7(nm ~ 0.14), $G_C = dI_C/dV_{CB}$ and the true hot-electron distribution are linearly scaled and are similar in shape. G_C curves for injection energies $qV_{BE} = 150$–170 meV are plotted in Fig. 4. A clear ballistic behavior is observed. The peak positions in G_C track exactly the injection energy qV_{BE} and are at $qV_{BE} - \Delta$ (the "ballistic condition") where $\Delta \sim 25$ meV (Ref. 6) is the displacement of the normal energy distribution peak below the Fermi level in the emitter (Fig. 1). The ballistic fraction of the electrons that cross the AlGaAs analyzer peak is estimated at about 30% of the injected current.

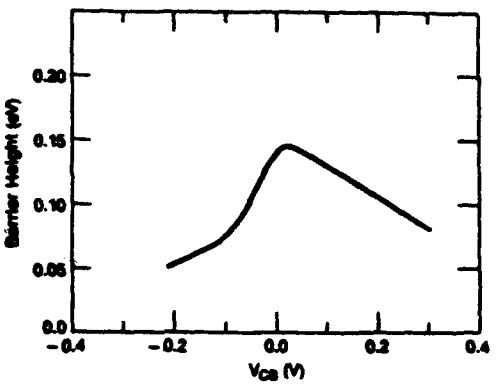

FIG. 3. Barrier height as a function of biasing voltage for an AlGaAs collector barrier, obtained by thermionic emission analysis of temperature-dependent current-voltage characteristics.

The ballistic transport maintains the phase coherence of the electrons and thus interference effects in the base can take place. This resulted in resonances in the tunneling currents into the base as shown in Fig. 5. The tunneling conductance is expected to reach a peak whenever the peak of the normal energy distribution, at $qV_{BE} - \Delta$, crosses the bottom

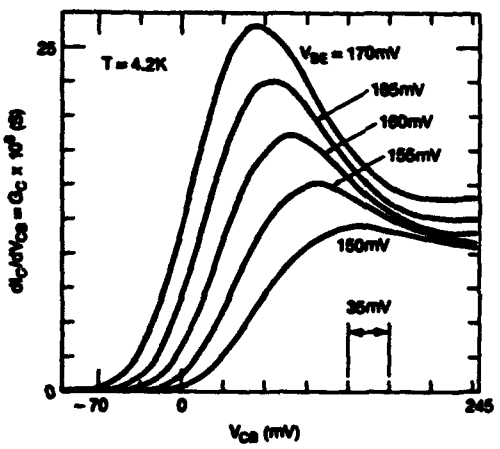

FIG. 4. Differential output conductance G_C as a function of the collector-base voltage. The parameter is the injection voltage V_{BE}. The value of G_C is proportional to the number of ballistic electrons.

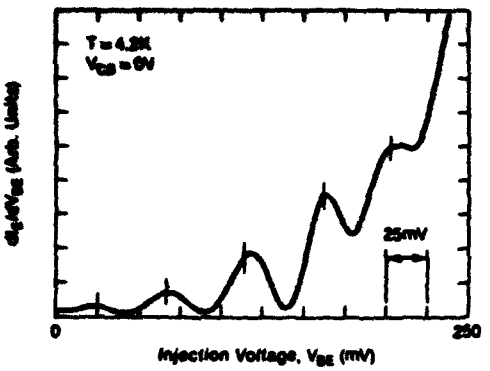

FIG. 5. Derivative of the measured injected current I_E with respect to base-emitter injection voltage V_{BE} for $V_{CB} = 0$ at 4.2 K. Each peak corresponds to a crossing of a subband minimum in the base. The calculated peak positions are marked by the vertical bars for comparison.

of a quasi-2D electron band formed in the base. We have estimated these conductance peak positions by solving the Schrödinger equation in the $In_{0.15}Ga_{0.85}As$ base assuming $m^* = 0.060m_e$, where m_e is the free-electron mass, and a nonparabolicity parameter $\alpha = 0.72$ eV^{-1} obtained from the virtual crystal approximation,[7] and noted them in Fig. 5. Even though this is not a self-consistent solution for the Poisson and Schrödinger equations,[8] it still gives a very good agreement with the experimental results. Note also that the observed strong peaks in Fig. 5 are another indication of the large fraction of ballistic electrons.

In summary, we report on the first successful demonstration of a pseudomorphic *n*-type InGaAs base THETA device. The maximum current transfer ratio was 0.89 at 4.2 K (0.87 at 77 K), and the minimum ballistic fraction was about 30%, detected by an energy spectroscopy technique. The relatively high gain was attributed mainly to the greater Γ-L energy separation.

The authors would like to acknowledge with gratitude T. W. Hickmott and S. Tozer for their help in the measurements. The work was partly supported by DARPA and administered by ONR, contract No. N00014-87-C-0709.

[1]M. Heiblum, I. M. Anderson, and C. M. Knoedler, Appl. Phys. Lett. 49, 207 (1986).
[2]M. Heiblum, M. I. Nathan, D. C. Thomas, and C. M.Knoedler, Phys. Rev. Lett. 55, 2200 (1985).
[3]M. Heiblum, E. Calleja, I. M. Anderson, W. P. Dumke, C. M. Knoedler, and L. Osterling, Phys. Rev. Lett. 56, 2854 (1986).
[4]T. W. Hickmott, P. M. Solomon, R. Fisher, and H. Morkoç, J. Appl. Phys. 57, 2844 (1985).
[5]K. Inoue, H. Sakaki, J. Yoshino, and Y. Yoshioka, Appl. Phys. Lett. 46, 973 (1985).
[6]M. Heiblum and M. V. Fischetti, "Ballistic Electron Transport in Hot Electron Transistors," to appear in *Physics of Quantum Electron Devices*, edited by F. Capasso, in *Topics in Current Physics* (Springer, Berlin, 1988).
[7]The conduction-band nonparabolicity is accounted for via $E(k) = (\hbar^2k^2/2m^*)(1 - \alpha\hbar^2k^2/2m^*)$, where $E(k)$ is the kinetic energy in the Γ band and α is the nonparabolicity parameter. The value for α in $In_{0.15}Ga_{0.85}As$ was approximated from a linear interpolation between $\alpha = 0.55$ eV^{-1} in GaAs and $\alpha = 1.167$ eV^{-1} in $In_{0.53}Ga_{0.47}As$.
[8]M. Heiblum, M. V. Fischetti, W. P. Dumke, D. J. Frank, I. M. Anderson, C. M. Knoedler, and L. Osterling, Phys. Rev. Lett. 58, 816 (1987).

Observation of Single-Optical-Phonon Emission

M. Heiblum, D. Galbi, and M. Weckwerth
IBM Research Division, Thomas J. Watson Research Center, Yorktown Heights, New York 10598
(Received 13 October 1988)

We report an observation of a single-optical-phonon emission by monoenergetic hot electrons traversing thin n^+-type GaAs and thin undoped AlGaAs layers in times much shorter than the classical phonon period. This was done by injecting ballistic electrons into the thin layers with energy around the threshold for optical phonon emission and monitoring their exit energy. We estimate a scattering time of $\approx$200 fsec for electrons with energy of about 85 meV in n^+-type GaAs, and $\approx$550 fsec for 40-meV electrons in undoped AlGaAs.

PACS numbers: 73.50.Gr, 63.20.Dj

Among the variety of phonons in GaAs, the longitudinal optical (LO) phonons are coupled most strongly to low-energy electrons. Electrons with wave vector $\mathbf{k}$ will scatter via phonons with wave vector $\mathbf{q}$ to $\mathbf{k}'$ ($\mathbf{q}=\mathbf{k}-\mathbf{k}'$) with a probability proportional to $|\mathbf{q}|^{-2}$ in unscreened material, thus preferring to maintain their original direction. The $\mathbf{q}=0$ LO phonon energy in GaAs has been measured via neutron scattering[1] and inelastic tunneling,[2] and is $\hbar\omega_{LO}\simeq 36$ meV. At low temperatures, when the phonon occupation number is small, scattering events are mostly due to phonon emission which is possible only when the electron energy exceeds the lowest unoccupied energy state by at least 36 meV. Using energy spectroscopy, Dimaria *et al.*[3] have observed phonon replicas in SiO_2 in electron distributions emerging into vacuum. Multiphoton emission in GaAs was observed by Shaw[4] via photoconductivity experiments, and more recently by Hickmott *et al.*[5] in tunneling experiments. We report here a direct observation of monoenergetic, ballistic, hot electrons that emitted a single LO phonon when traversing very thin layers of n^+-type GaAs and insulating AlGaAs. It is particularly interesting that the transit time of the electrons through the layers is smaller than the phonon classical period ($2\pi/\omega_{LO}$).

To observe the emission of a phonon by a hot electron, a potential barrier (spectrometer) was constructed; its height was considerably lower than $\hbar\omega_{LO}$ to enable electrons with energy less than $\hbar\omega_{LO}$ to pass, but sufficiently high to prevent those hot electrons that lost $\hbar\omega_{LO}$ from passing. A quasi monoenergetic hot-electron beam was produced by a tunnel barrier (injector), which was made especially wide in order to achieve an energetically narrow hot-electron beam. Our hot-electron structures, described in Fig. 1, were grown by molecular-beam epitaxy, were composed of n^+-type GaAs emitter, undoped AlGaAs tunnel barrier injector, n^+-type GaAs transport region (base), undoped AlGaAs spectrometer barrier, and n^+-type GaAs collector layer.[6,7] The spectrometer barrier, 70 nm thick, with AlAs mole fraction $x=7\%$, had a conduction-band discontinuity of 63 meV. Because of some 1×10^{16}-cm^{-3} unintentional negative charges in all our molecular-beam-epitaxy layers,[8] the measured barrier height was about 73 meV (the additional 10-meV bowing is expected to have a potential maximum at the center of the barrier). With doping of 8×10^{17} cm^{-3} in all n^+-type GaAs layers and Fermi energy of 45 meV at 4.2 K, the spectrometer potential height above the Fermi level in the base was $\Phi_C=73-45=28$ meV. The barrier height was measured by observing the onset of the collector current as will be shown later. For our thick injector tunnel barrier, 50 nm thick with $x=7\%$, the expected full width at half maximum of the injected energy distribution is about 4 meV.[6,7]

Applying $V_{CB}\geq 30$ meV across the spectrometer barrier, reduces its potential peak to 63 meV (by flattening the bowing potential) and shifts its position to the base side (flat-band conditions as seen in Fig. 1). A further increase in V_{CB} affects Φ_C only slightly. This assures that a large enough window Δ exists between the phonon

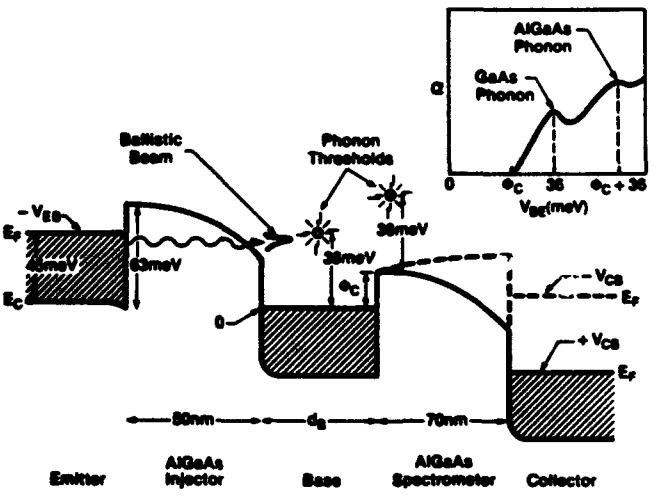

FIG. 1. The conduction band in the hot-electron structure with the expected ballistic electron distribution and the different thresholds for phonon emission. Inset: The expected behavior of α, as a result of phonon emission in GaAs and in AlGaAs.

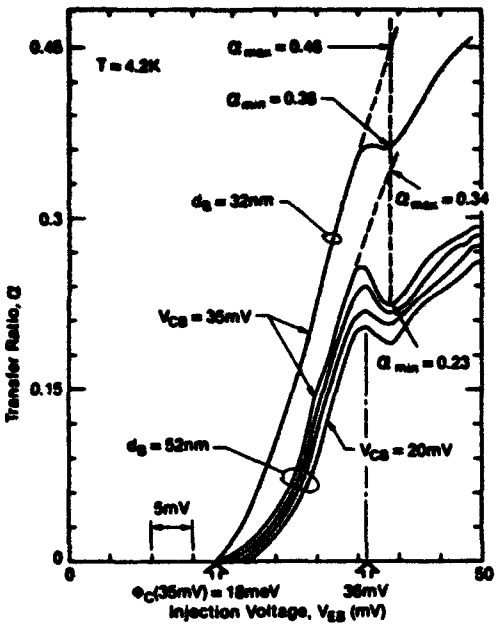

FIG. 2. The transfer ratio α curves for different V_{CB}'s (5-mV steps) in the 52-nm base device. As V_{CB} increases, the window between the phonon emission threshold and the collector barrier height increases and α experiences a stronger dip. The α measured in the 32-nm base device at V_{CB} = 35 mV is also shown.

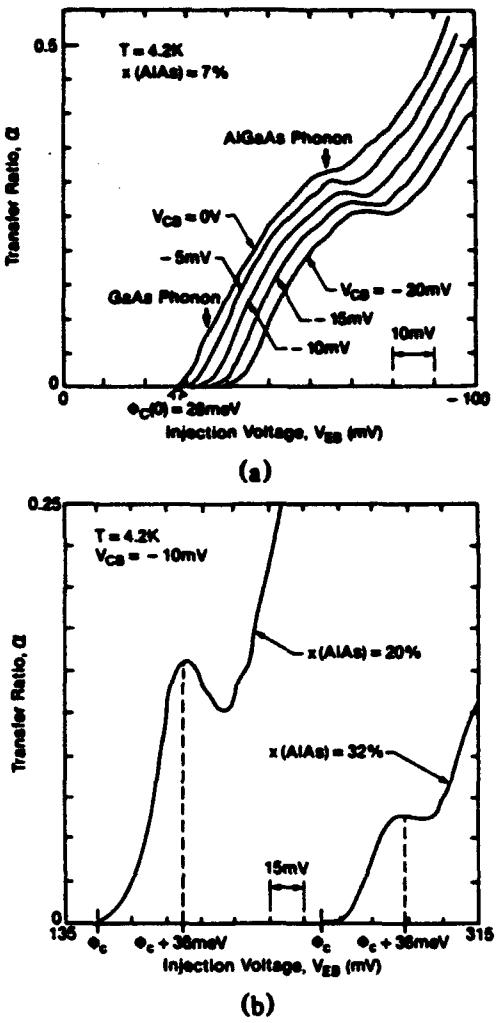

FIG. 3. The transfer ratio α exhibiting the phonon emission in $Al_xGa_{1-x}As$, for (a) x = 7%, and for (b) x = 20% and 32%. Note in (a) how the phonon-related loss peak in the AlGaAs builds up as V_{CB} becomes slightly negative.

threshold and the barrier top [$\Delta = \hbar\omega_{LO} - \Phi_C = 36 - (63 - 45) = 18$ meV], allowing the full width of the ballistic distribution, injected by the tunnel barrier, to surmount the spectrometer barrier before emitting a phonon. We have looked at the *differential transfer ratio,* defined as $\alpha = dI_C/dI_E$ for V_{CB} = const, where I_C and I_E are the collected and emitted (injected) currents, as a function of the injection voltage, V_{EB}. The quantity α is a good measure of the electron loss since it eliminates constant leakage currents and normalizes the collected current to the injected current (which rises rapidly with the injection voltage).

In Fig. 2 we show the behavior of α for structures with base widths of 52 and 32 nm, for different spectrometer biasing voltages $V_{CB} > 0$. We see that α rises rapidly when the injection energy eV_{EB} exceeds the barrier height, Φ_C [$\Phi_C(0) = 28$ meV for $V_{CB} = 0$, as seen in Fig. 3(a)]. When $eV_{EB} = 36$ meV, the LO phonon energy α drops sharply, reaching a minimum around 40 meV and thereafter increases again. The drop in α beyond $V_{EB} = 36$ mV is due to those ballistic electrons that emitted a phonon. The overall monotonic rise of α is determined by the energy dependence of all scattering mechanisms, and in particular the quantum-mechanical reflections from the base-spectrometer interface, dominant for energies close to the spectrometer potential height. We define the fractional loss of electrons at energy E due to phonon emission as $\alpha_{min}(E)/\alpha_{max}(E)$, where $\alpha_{min}(E)$ is the measured $\alpha(E)$, and $\alpha_{max}(E)$ is the extrapolated $\alpha(E)$ as if phonon emission did not occur, as seen in Fig. 2. The different slopes of $\alpha(E)$ before and after threshold indicate an increase in the scattering rate as the electron energy increases. To minimize the error in our estimate for the scattering rates deduced from the extrapolated $\alpha_{max}(E)$, we measure $\alpha_{min}/\alpha_{max}$ at the lowest possible energy above threshold, namely, about a distribution width above the threshold energy. As V_{CB} increases, Φ_C decreases (indicated by the shifting onsets of α in Fig. 2), and the ballistic window Δ increases (up to about 18 meV as shown before), followed in turn by an increase of $\alpha_{min}(E)/\alpha_{max}(E)$. We find that increasing V_{CB} above 35 mV does not increase Δ and $\alpha_{min}(E)/\alpha_{max}(E)$ any more.

We estimate the mean free path λ from Fig. 2 using $\exp(-d_B/\lambda) = \alpha_{min}(E)/\alpha_{max}(E)$, where d_B is the base width. At an energy of about 85 meV we find $\lambda \simeq 126$ nm and $\lambda \simeq 130$ nm for the structures with base width of 52 and 32 nm, respectively. Since at 85 meV the ballis-

tic electron velocity is about 6.1×10^7 cm/sec (assuming a band-edge effective electron mass of $0.067m_e$ and a nonparabolicity parameter $\beta=-0.834$/eV),[9] the deduced scattering time for phonon emission τ at 85 meV is about 210 fsec in the n^+-type GaAs layers. At slightly higher energies, say 90 meV, we find $\lambda\simeq115$ nm and $\tau\simeq185$ fsec. It is interesting to note that our results are in approximate agreement with experiments done in unscreened GaAs layers.[10] We compare our results with the theoretical predictions for the LO phonon emission rate in undoped GaAs.[11] In mks units,

$$\frac{1}{\tau(E)}=\frac{e^2m^{1/2}\hbar\omega_{LO}}{4\sqrt{2}\pi\hbar^2E^{1/2}}\left[\frac{1}{\epsilon_\infty}-\frac{1}{\epsilon_{DC}}\right](1+n_{LO})F(E,E'). \tag{1}$$

Here,

$$F(E,E')=\frac{1}{C}\left[A\ln\frac{\gamma^{1/2}(E)+\gamma^{1/2}(E')}{\gamma^{1/2}(E)-\gamma^{1/2}(E')}+B\right],$$

$\gamma(E)=E(1-\beta E)$, $E'=E-\hbar\omega_{LO}$, n_{LO} is the phonon occupation number, $\epsilon_{DC}=12.9\epsilon_0$ and $\epsilon_\infty=10.9\epsilon_0$ are the static and optical dielectric constants of GaAs and ϵ_0 is the permitivity of free space, A, B, and C are factors due to nonparabolicity effects (in parabolic bands $A=C=1$ and $B=0$), and $m=0.067m_e$. Substituting in Eq. (1) $n_{LO}=0$ at $T=4.2$ K, $E=85$ meV, $E'=49$ meV, and calculating[11] $A=5.5$, $B=-0.52$, and $C=5.3$, we find $\tau=240$ fsec.

This excellent agreement with our measured τ is somewhat surprising since at our equilibrium electron concentration of 8×10^{17} cm^{-3} the $q=0$ LO phonons and plasmons have similar energies ($\hbar\omega_p\simeq38$ meV), and thus interact strongly, resulting in two coupled modes: a plasmonlike mode with $q=0$ energy $\hbar\omega_+(0)=43$ meV and a phononlike mode with $\hbar\omega_-(0)=28$ meV (Ref. 12). The lowest possible $|q|$ modes for which scattering is most dominant in unscreened GaAs is

$$q_{min}=|k(85\text{ meV})|-|k'(49\text{ meV})|\simeq1\times10^6\text{ cm}^{-1},$$

and $q_{min}/k_F\simeq0.35$, where k_F is the Fermi wave vector. Because of dispersion, we would expect to observe two thresholds, one at $\hbar\omega_+(0.35)\simeq57$ meV and the other at $\hbar\omega_-(0.35)\simeq31$ meV (Ref. 12), both are not observed. Screening might be rather important since $k_0>|q_{min}|$, where $1/k_0$ is the Thomas-Fermi screening length. Then emission of higher q LO phonons with $\hbar\omega_{LO}\simeq36$ meV can dominate due to their high density, explaining the 36-meV peak. Since the coupling to the plasmon branch is expected to be strong,[12] the absence of an observed threshold at 57 meV is not clear. The higher q, higher frequency, plasmons modes, however, are heavily damped by single-electron excitations, and thus not observable. Quantization effects in the narrow base are less likely to affect our observations due to the similarity of the results found in the 52- and 32-nm-wide bases. However, the possibility of an emission of an unscreened, uncoupled, LO phonon, in agreement too with our observations should not be ruled out.

The same structure enabled us also to observe single-phonon scattering events in AlGaAs. In the spectrometer barrier, when the ballistic hot electrons lose energy and relax to the bottom of the conduction band, they can "roll back" to the base or "roll forward" to the collector, depending on the potential shape in the barrier. Indeed, for $V_{CB}>0$ it is difficult to verify the existence of electron scattering in AlGaAs, since both the ballistic electrons and the ones that scatter reach the collector. However, when a small negative bias is applied across the barrier (−10 to −20 mV), a clear peak in α is observed near $eV_{EB}=\Phi_C+36$ meV,[13] as we show in Fig. 3(a) (the GaAs-like LO phonon is 35.5 meV in AlGaAs with $x=7\%$). Here the estimate for λ is cruder since it is more difficult to determine accurately the traversal region in the AlGaAs barrier (see dotted line in Fig. 1). At higher negative bias, the threshold voltage is not unique and the phonon threshold broadens and shifts to higher energies. We have used the same method as before to estimate λ. Using an estimated length to the potential peak of 45 nm for $V_{CB}=-10$ mV (via a Poisson solution) and an excess energy in the AlGaAs of $\simeq40$ meV, we find $\lambda\simeq230$ nm. With an estimated average ballistic velocity of 4.2×10^7 cm/sec in the barrier, we arrive at $\tau=550$ fsec. Using in Eq. (1) $E=40$ meV, $E'=4$ meV, and the appropriate parameters for $Al_{0.07}Ga_{0.93}As$,[14,15] we find $\tau\simeq490$ fsec, which is in good agreement with our measurements.

Phonon emission can also be observed in AlGaAs layers with higher AlAs mole fractions. We have fabricated similar hot-electron structures but with $x=20\%$ and 32% in the barriers. Here, an electron energy in the GaAs base must be at least some 180 and 290 meV, respectively, to enter the AlGaAs spectrometer; however, in AlGaAs the electron energy can be near the phonon emission threshold. Figure 3(b) shows the α of these two devices for a small negative spectrometer voltage, $V_{CB}=-10$ mV. Again, the peaks in α are very near 36 meV above Φ_C, resolving clearly the GaAs-like LO phonons (which are about 35 and 34.3 meV in AlGaAs with $x=20\%$ and 32%, respectively[14,15]). The AlAs-like phonons, being 44.6 and 47 meV, respectively, are difficult to resolve since the ballistic distributions at high injection energies in these structures are much broader ($\simeq60$ meV, Ref. 7). Since the energy width of the ballistic distributions here is wider than the window $\Delta\simeq36$ meV, and its width requires an extrapolation too long for an accurate determination of $\alpha_{max}(E)$, the validity of α as a quantitative measure of electron loss is questionable. If we assume the dominant scattering to be due to the GaAs-like LO phonons and $E=40$ meV, Eq. (1) predicts $\tau=400$ fsec in AlGaAs with $x=25\%$, and a λ of about 150 nm.

In summary, we have directly observed electrons that emitted a single longitudinal optical phonon in n^+-type GaAs and in undoped AlGaAs layers. In both layers a clear single threshold at 36 meV (the LO phonon energy) was observed, and we have estimated the phonon-related scattering time near threshold to be $\simeq$200 fsec in n^+-type GaAs.

We would like to thank L. Osterling for his help with the molecular-beam-epitaxy growth, M. V. Fischetti and J. A. Kash for helpful discussions, and W. D. Dumke, T. W. Hickmott, A. B. Fowler, J. Imry, C. J. Kircher, U. Meirav, P. J. Price, K. Seo, and F. Stern for useful comments on the manuscript. The work was partly supported by the U.S. Defense Advanced Research Projects Agency and administered by the ONR, Contract No. N00014-87-C-0709.

[1]J. L. T. Waugh and G. Dolling, Phys. Rev. 132, 2410 (1963).

[2]R. N. Hall, J. H. Racette, and H. Ehrenreich, Phys. Rev. Lett. 4, 456 (1960).

[3]D. J. Dimaria, M. V. Fischetti, J. Batey, L. Dori, E. Tierney, and J. W. Stasiak, Phys. Rev. Lett. 57, 313 (1986).

[4]R. W. Shaw, Phys. Rev. B 3, 3283 (1970).

[5]T. W. Hickmott, P. M. Solomon, F. F. Fang, F. Stern, R. Fischer, and H. Morkoç, Phys. Rev. Lett. 52, 2053 (1984).

[6]M. Heiblum, Solid State Electron. 24, 343 (1981).

[7]M. Heiblum, M. I. Nathan, D. C. Thomas, and C. M. Knoedler, Phys. Rev. Lett. 55, 2200 (1985).

[8]T. W. Hickmott, P. M. Solomon, R. Fischer, and H. Morkoç, J. Appl. Phys. 57, 2844 (1985).

[9]M. Heiblum, M. V. Fischetti, W. P. Dumke, D. J. Frank, I. M. Anderson, C. M. Knoedler, and L. Osterling, Phys. Rev. Lett. 58, 816 (1987).

[10]J. A. Kash, J. C. Tsang, and J. M. Hvam, Phys. Rev. Lett. 54, 2151 (1985). They had measured an average scattering time of 165 fsec per scattering for 0.5-eV hot electrons in unscreened thick GaAs layers.

[11]W. Fawcett, A. D. Boardman, and S. Swain, J. Phys. Chem. Solids 31, 1963 (1970).

[12]M. E. Kim, A. Das, and S. D. Senturia, Phys. Rev. B 18, 6890 (1978).

[13]Φ_C was determined accurately by measuring the exact onset of the collector current as a function of V_{EB} (not shown here).

[14]Benard Jusserand and Jacques Sapriel, Phys. Rev. B 24, 7194 (1981).

[15]S. Adachi, J. Appl. Phys. 58, 1 (1985).

High-Gain Pseudomorphic InGaAs Base Ballistic Hot-Electron Device

K. SEO, MORDEHAI HEIBLUM, SENIOR MEMBER, IEEE, C. M. KNOEDLER, J. E. OH, J. PAMULAPATI, AND PALLAB BHATTACHARYA, FELLOW, IEEE

Abstract—We report on a high-gain ballistic hot-electron device. The GaAs–AlGaAs heterostructure device, with a 21-nm-thick pseudomorphic $In_{0.12}Ga_{0.88}As$ base, had a current gain of 27 at 77 K and 41 at 4.2 K. As characteristically seen in ballistic devices, transfer into the L valleys limited the maximum gain. The Γ-L valley separation in the strained $In_{0.12}Ga_{0.88}As$ was estimated to be about 300 meV.

WE HAVE recently reported on the dc performance of a ballistic pseudomorphic InGaAs base, tunneling hot-electron transfer amplifier (THETA) device [1]. With our research on GaAs base devices [2], [3], we have found that most scatterings [4], such as electron–plasmon and electron–electron in the n-doped base, are relatively small in thin and nonheavily doped base devices, but scattering to the L valleys is severe and limits the maximum possible current gain. For GaAs base devices, by reducing the AlGaAs collector barrier height and increasing the available window for ballistic transport (between collector barrier top and L valleys bottom), a maximum current transfer ratio $\alpha_M = 0.9$ (and a current gain of 9) were achieved [2]. In pseudomorphic InGaAs base devices the intervalley energy separation $E_{\Gamma L}$ is larger and so is the band discontinuity between InGaAs and AlGaAs, thus allowing a lower AlAs mole fraction in the barriers and a wider energy window without excessive leakage currents. We have previously reported a gain of 9 in a heavily doped pseudomorphic $In_{0.15}Ga_{0.85}As$ base device, having also a high collector breakdown voltage [1]. Recently, Hase *et al.* [5] have reported on the characteristics of a THETA device with an $In_{0.2}Ga_{0.8}As$ 30-nm-thick base. However, the base thickness exceeded the critical layer thickness [6] for a pseudomorphic layer, as evidenced by the very large voltages required in the structure. Here, we report a dramatic improvement in the current gain of a pseudomorphic InGaAs base device resulting from a reduction in the base thickness and doping and the enlargement of the energy window. We have measured current gains as high as 41 in the new devices.

The InGaAs pseudomorphic structures were grown by molecular beam epitaxy on (100) n^+ GaAs substrates. Fig. 1 describes the energy-band diagram of the device under normal bias conditions in a common-base configuration (CBC). The tunnel injector on the left is formed from a thin $Al_xGa_{1-x}As$ layer (10 nm, undoped, $x = 0.28$) which is sandwiched between an n^+ GaAs emitter and a strained n^+ $In_yGa_{1-y}As$ base (21 nm, $y = 0.12$) doped to 7×10^{17} cm^{-3}. Another undoped $Al_zGa_{1-z}As$ layer between the base and an n^+ $In_{0.12}Ga_{0.88}As$ collector layer forms the collector barrier (65 nm, $z = 0.1$, and graded on the base side to $z = 0$ over 10 nm to reduce the quantum mechnical reflections for the incoming hot electrons). This barrier prevents the equilibrium electrons in the base from entering the collector. The 10-nm-thick $In_{0.12}Ga_{0.88}As$ collector layer was merged with the underlying n^+ GaAs buffer and substrate by compositional grading. The emitter area of the device was 16×18 μm^2.

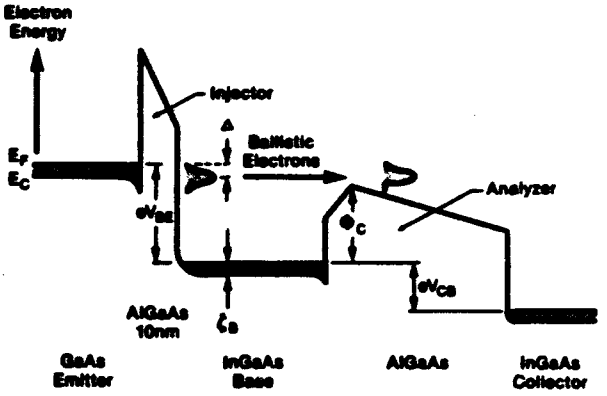

Fig. 1. Schematic diagram of the conduction band of a THETA device under forward-bias operation.

Output characteristics, I_C–V_{CB}, in a CBC, measured at 77 K, with I_E as a parameter, are shown in Fig. 2(a). I_C and I_E are the collector and emitter currents, and V_{CB} is the collector–base voltage. The high output conductance is due to the wide graded region of the collector barrier, leading to a reduction of the barrier height as V_{CB} increases. Even for 10 percent AlAs mole fraction in the collector barrier, the collector breakdown voltage is near 0.3 V due to the increased conduction-band discontinuity. This can be verified by measuring the differential current transfer ratio $\alpha = dI_C/dI_E$ versus V_{BE} at $V_{CB} = 0$, as shown with the dashed lines in Fig. 2(b). At the onset of α (or the collector current) the emitter Fermi level crosses the collector barrier peak, and eV_{BE} at the onset determines the collector barrier height above the Fermi level in the base (128 meV). Using 45 meV for the Fermi energy in the base, we find a collector barrier height of 173 meV. In a similar device but

Manuscript received September 27, 1988. This work was supported in part by DARPA and administered by ONR under Contract N00014-87-C-0709.

K. Seo, M. Heiblum, and C. M. Knoedler are with the IBM Research Division, Thomas J. Watson Research Center, Yorktown Heights, NY 10598.

J. E. Oh, J. Pamulapati, and P. Bhattacharya are with the Department of Electrical Engineering and Computer Science, University of Michigan, Ann Arbor, MI 48109.

IEEE Log Number 8826123.

0741-3106/89/0200-0073$01.00

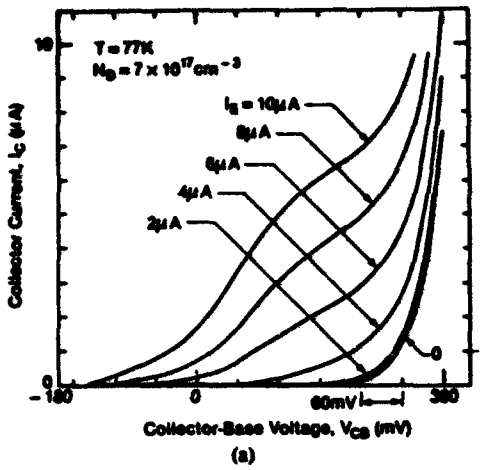

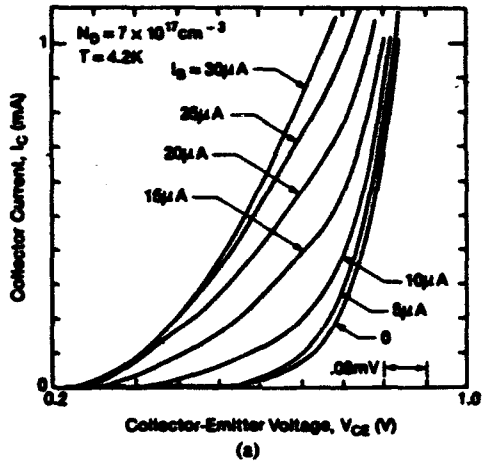

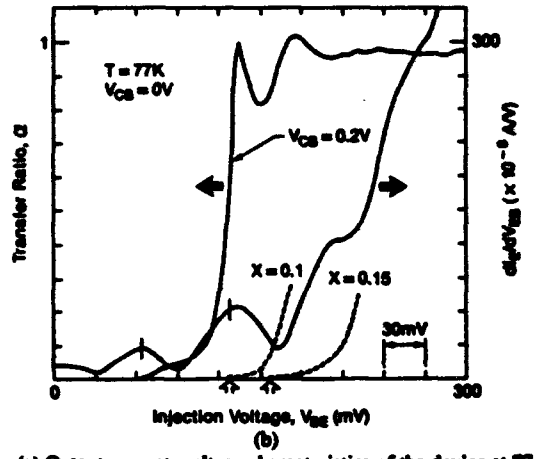

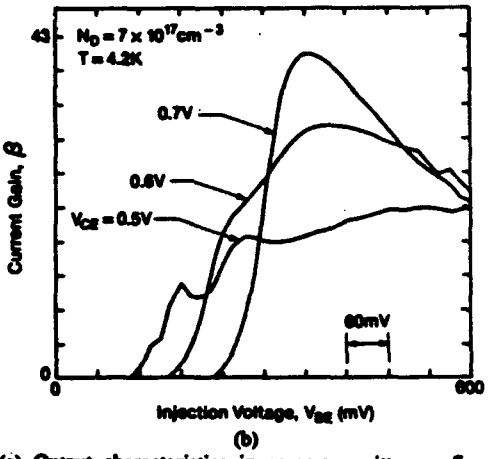

Fig. 2. (a) Output current–voltage characteristics of the device at 77 K. The parameter is the injection current I_B. (b) Differential current gain α and the derivative of the emitter current versus the injection voltage V_{BE}, measured at 77 K. Plotted also are the onsets of the α's of the same device and another with x(AlAs) = 15 percent for V_{CB} = 0 (dotted lines). Calculated peak positions in the emitter conductance are marked by the vertical bars.

Fig. 3. (a) Output characteristics in common-emitter configuration. (b) Current gain in this configuration as a function of the injection voltage, reaching a maximum of 41 at the threshold for L valley transfer.

with x(AlAs) = 15 percent (also shown in Fig. 2(b)), a barrier height of 213 meV is determined. Using the conduction-band discontinuity $\Delta E_C = 0.67\Delta E_G$ [2], [7] for GaAs/AlGaAs heterostructure, we get ΔE_C between $In_{0.12}Ga_{0.88}As$ and GaAs of some 90 meV, or 7.5 meV/1 percent of InAs. For V_{CB} = 0.2 V, the device shows a rather uniform $\alpha \sim 0.97$, with strong resonance peaks that reach unity. Note that α near its onset rises rapidly over about 60–80 meV, a characteristic feature of ballistic distributions ~60 meV wide [8]. The resonances in α are due to the "virtual states" in the thin quantum-well base [9], resulting from interference effects of the ballistic electrons passing over the collector barrier (small quantum mechanical reflections from the collector barrier form these states). These resonances are also visible in the tunneling currents injected into the base, as shown in the derivative of I_E with respect to V_{BE} in Fig. 2(b). For $m^* = 0.061m_e$, where m_e is the free electron mass, the peak positions agree fairly well with the quasi two-dimensional subband energies calculated for a square well base [1] (see Fig. 2(b)). Note that the strong peaks observed also indicate a large fraction of ballistic electrons.

We attribute the high α particularly to the large Γ–L energy separation $E_{\Gamma L}$. The typical drop commonly observed in α when the injection energy exceeds $E_{\Gamma L}$ [3] was difficult to observe here due to the thin base. However, a distinctive reduction was observed in the differential current gain in a common-emitter configuration (CEC), $\beta = dI_C/dI_B$, where I_B is the base current. The output charcteristics of the device in CEC are shown in Fig. 3(a), exhibiting a rather high output conductance. β is plotted in Fig. 3(b) as a function of V_{BE} where V_{CE} is a parameter. The transfer to the L valleys can be clearly identified when β reaches a maximum and subsequently drops sharply. β reaches a maximum of 41 at V_{CE} = 0.7 V and V_{BE} = 360–365 mV (at 77 K, β_{max} = 27 at the same applied voltages). A simple exponential dependence of the static current gain (I_C/I_B) on the base thickness leads to a mean-free path (mfp) for ballistic transport larger than 500 nm at 4.2 K just below the threshold for L valley transfer. A similar device but with heavier doping in the base (1×10^{18} cm^{-3}) and 15 percent AlAs mole fraction in the collector barrier had a maximum current gain of 17 at 77 K and 21 at 4.2 K (a mfp of some 360 nm). We attribute the resultant long mfp's to the quasi two-dimensional nature of the base, thus leading to reduced scattering events [10]. $E_{\Gamma L}$ can be found by adding the Fermi energy (45 meV) to the threshold (360–365 meV), and subtracting an LO zone edge phonon energy (28

meV) [3]. This leads to $E_{\Gamma L} \simeq 380$ meV in the strained $In_{0.12}Ga_{0.88}As$ (we have found before $E_{\Gamma L} = 410$ meV in strained $In_{0.15}Ga_{0.85}As$ layers [1]).

To conclude, with the introduction of the InGaAs pseudomorphic base in a ballistic hot-electron device, high gain (41 at 4.2 K), attributed mainly to a large Γ–L energy separation ($\simeq$ 380 meV), was realized. Further increase in the Γ–L energy separation might enable even higher gains. The devices exhibit strong quantum size effects due to the large fraction of ballistic electrons traversing the 21-nm base.

References

[1] K. Seo, M. Heiblum, C. M. Knoedler, W. P. Hong, and P. Bhattacharya, "Pseudomorphic InGaAs base ballistic hot electron device," *Appl. Phys. Lett.*, vol. 53, p. 1946, 1988.

[2] M. Heiblum, I. M. Anderson, and C. M. Knoedler, "dc performance of ballistic tunneling hot-electron transfer amplifiers," *Appl. Phys. Lett.*, vol. 49, p. 207, 1986.

[3] M. Heiblum *et al.*, "Evidence of hot-electron transfer into an upper valley in GaAs," *Phys. Rev. Lett.*, vol. 56, p. 2854, 1986.

[4] A. P. Long, P. H. Beton, and M. J. Kelly, "Hot-electron transport in heavily doped GaAs," *Semocond. Sci. Technol.*, vol. 1, p. 63, 1986.

[5] I. Hase *et al.*, "Strained GaInAs-base hot electron transistor," *Electron. Lett.*, vol. 24, p. 279, 1988.

[6] I. J. Fritz, P. L. Gourley, and L. R. Dawson, "Critical layer thickness in $In_{0.2}Ga_{0.8}As$/GaAs single strained quantum well structures," *Appl. Phys. Lett.*, vol. 51, p. 1004, 1987.

[7] M. Heiblum *et al.*, "Electron interference effects in quantum wells: Observation of bound and resonant states," *Phys. Rev. Lett.*, vol. 58, p. 816, 1987.

[8] G. Ji *et al.*, "Determination of band offsets in AlGaAs/GaAs and InGaAs/GaAs multiple quantum wells," *J. Vac. Sci. Technol. B*, vol. 5, p. 1346, 1987.

[9] M. Heiblum, M. I. Nathan, D. C. Thomas, and C. M. Knoelder, "Direct observation of ballistic transport in GaAs," *Phys. Rev. Lett.*, vol. 55, p. 2200, 1985.

[10] D. C. Herbert, "Structured-base hot-electron transistors: 1. Scattering rates," *Semicond. Sci. Technol.*, vol. 3, p. 101, 1988.

Inert gas reactive ion etching damage to GaAs using inverted heterojunctions

C. M. Knoedler, L. Osterling, and M. Heiblum
IBM T. J. Watson Research Center, Yorktown Heights, New York 10598

(Received 12 September 1988; accepted for publication 24 October 1988)

Selectively doped inverted heterojunctions containing a two-dimensional electron gas were used as a sensitive vehicle for monitoring dry processing damage. We found that the electron sheet concentration, strongly dependent on the total number of carriers in the GaAs cap layer, and the mobilities were significantly depressed even for very short exposures to low-voltage helium plasmas. Argon, which caused less degradation than helium, was found to increase the sheet carrier concentration and hence the mobility after prolonged exposure. The damage mechanism responsible for the carrier loss in both cases is most likely the production of traps. The subsequent carrier increase seen for the argon case is probably attributable to the creation of a very thin donorlike damage layer on the surface of the GaAs cap layer.

GaAs/AlGaAs heterostructure devices are susceptible to electrical damage caused by dry etching.[1] The damage becomes more evident as the epitaxial layers are reduced in thickness. The tunneling hot-electron transfer amplifier (THETA) device,[2] whose base dimensions have decreased by 80% since first fabricated, experiences carrier depletion after reactive ion etching (RIE) at low dc self-bias voltages. Previous work[3] related the carrier depletion in the base layer of the device to overetching at an etch stop layer. That study, however, did not explore the role of the inert buffer gas in causing damage. While other work[4,5] did study the effect of inert gas ion damage on GaAs, this communication examines the particular effect of low-voltage inert gas plasmas on the sheet carrier concentration and electron mobility in heterostructures.

The selectively doped inverted heterojunction (SDIH)[6] samples used for this study were grown by molecular-beam epitaxy (MBE). An undoped GaAs buffer layer, grown on a semi-insulating GaAs (100) substrate, is followed by a thick (85.6 nm) $Al_{0.2}Ga_{0.8}As$ spacer layer. This spacer prevents the formation of a two-dimensional electron gas (2DEG) in the GaAs buffer layer. A 10-nm-thick layer of n^+-type ($1\times10^{18}/cm^3$) Si-doped $Al_{0.2}Ga_{0.8}As$ followed by a 6-nm, undoped $Al_{0.2}Ga_{0.8}As$ spacer layer comes next. The structure is completed with a 100-nm, undoped GaAs layer and a 32-nm n^+-type ($1\times10^{18}/cm^3$) GaAs cap layer. This GaAs/AlGaAs heterostructure, which serves as the diagnostic tool in this study, has a single 2DEG located in the GaAs on top of the AlGaAs layer. In this type of structure, the 2DEG concentration at the GaAs/AlGaAs interface is critically dependent on the number of carriers in the GaAs cap layer.

Square ($100\times100\,\mu m^2$) van der Pauw[7] patterns, lithographically defined and mesa etched on the heterostructure, had ohmic contacts [AuGe(120 nm)/Ni(20 nm)/Au (200 nm)] alloyed at 450 °C to the edges of the squares. After chemical or inert gas ion etch processing, van der Pauw squares were mounted on headers and bonded at a temperature of 160 °C. The Hall mobility, measured on as-grown samples at 77 K in the dark, was 34 400 $cm^2/V\,s$ with a sheet carrier concentration of $6.7\times10^{11}/cm^2$. The solid dots in Fig. 1 represent these results.

The samples used as a baseline for the experiment had their cap layers etched in a 3:1:50 phosphoric acid etch (phosphoric acid: hydrogen peroxide: water) maintained at 0 °C. This etch removes 30 nm of GaAs per minute. Etch times ranged from 5 to 30 s. The 5-s etch samples displayed a decrease in the number of 2DEG carriers and a slight increase in the mobility. This suggests some parallel conduction in the as-grown heterostructure. The other chemically etched samples showed reduced sheet carrier concentrations as well as decreased mobility as more of the cap layer was removed. The solid triangles in Fig. 1, with the etch times listed next to each point, represent these data.

The decrease in sheet carrier concentration with the reduction in cap layer thickness is attributable to the systematic removal of carriers from this layer which caused an increase in the depletion layer width at the surface. Simple modeling results, using a heterostructure simulator which solves the one-dimensional (1D) Poisson's equation for the potential and uses Fermi–Dirac statistics to determine the charge, show a reduction in carrier concentration with a decrease in cap layer thickness. Plotted as a line in Fig. 2(a) is

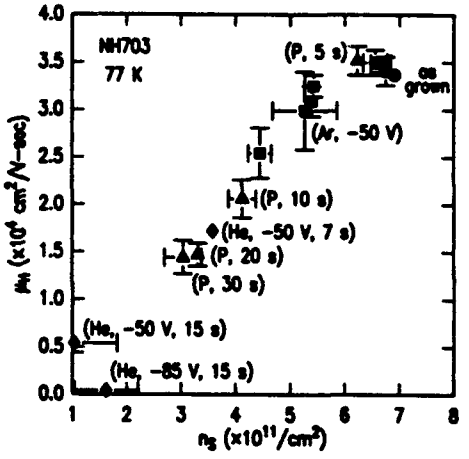

FIG. 1. Hall mobility plotted vs carrier concentration for the as-grown samples: (●), the phosphoric acid etched, baseline samples (▲), the helium exposed samples (◆), and the argon exposed samples (■). Note that the experimental points tend to lie on a line running diagonally through the figure.

 0021-8979/89/041800-03$02.40

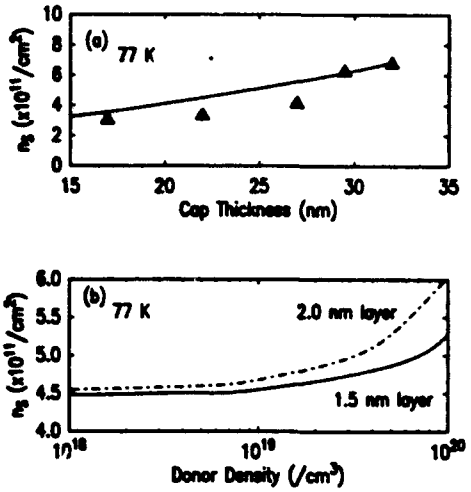

FIG. 2. Simulation results for a SDIH structure at 77 K. (a) The sheet carrier concentration as a function of the GaAs cap layer thickness is plotted as a line. The solid triangles are the experimental data points derived from the phosphoric acid etch results. (b) Plot of the increase in the sheet carrier concentration as the density of donorlike traps is increased within a thin (1.5 and 2.0 nm) surface layer of the GaAs cap.

the data derived from this simulation which qualitatively agree with the phosphoric acid etch data plotted as solid triangles. The decrease in mobility is directly related to the decrease in sheet carrier concentration because of the screening effect produced by the electron gas. A density reduction in this electron gas results in increased scattering and a subsequent mobility decrease.

The SDIH van der Pauw squares, subjected to helium and argon plasmas under RIE-like conditions, helped to quantify the electrical damage caused by the inert gases. The reactive ion etching system is a conventional, parallel plate reactor described elsewhere.[3,8] The van der Pauw samples were first exposed to a helium plasma under conditions similar to those used to etch the THETA devices. These conditions include a flow rate of 6 sccm, a pressure of 15 mTorr, a dc self-bias voltage of -85 V, a power density of 0.03 W/cm^2, and an exposure time of 15 s. Although no measurable etching of the heterostructure surfaces took place, these samples showed extensive reductions in sheet carrier concentration and mobility. A dc self-bias voltage of -50 V, at a pressure of 15 mTorr, a power density of 0.01 W/cm^2, and plasma exposure times of 7 and 15 s were the next set of helium parameters. The sheet carrier concentration and mobility were low but not to the extent of the -85 V case. The results for these samples, plotted as solid diamonds in Fig. 1, lie approximately on a line with the results for the chemically etched samples.

The van der Pauw surfaces exposed to an argon plasma at a flow rate of 6 sccm, a pressure of 15 mTorr, a dc self-bias of -50 V, and a power density of 0.01 W/cm^2 for times ranging from 10 to 40 s displayed less degradation. Figure 1 shows the argon data, plotted as solid squares, clustering between and approximately on a line with the 5- and 10-s phosphoric acid etch results. The sheet carrier concentrations and mobilities are slightly less than the as-grown samples, however these quantities both increase as the plasma exposure time increases.

The experimental data points, for the most part, lie along a line that runs diagonally through Fig. 1. This suggests that the mechanism for the sheet carrier concentration and mobility decrease in the ion exposed samples is similar to that in the chemically etched baseline samples. This mechanism is carrier loss in the cap layer. In the chemically etched samples, carriers are systematically removed from the cap layer. The generation of traps by ions and photons[9] that compensate the dopant in the GaAs cap layer appears to be responsible for the carrier loss in the plasma exposed samples. Trap generation induced in GaAs has been observed and characterized for various dry etching techniques.[10]

The experimental results indicate that the low-voltage helium and argon plasmas affect the heterostructure samples differently. The helium damage (-50 V and 7 s) is equivalent to the removal of carriers from the cap layer and reduces the number of carriers in the 2DEG by about 3×10^{11}/cm^2. A 15-s exposure results in a loss of about 5×10^{11}/cm^2 carriers. Argon, after an initial loss of about 2×10^{11}/cm^2 carriers, shows an increase in carrier concentration and mobility with increased exposure times. Figure 3 shows an expanded view of the argon data from Fig. 1. Listed beside each point is the plasma exposure time. A probable explanation for the carrier increase in the 2DEG is the creation of a high density of donorlike traps at the surface of the GaAs cap layer by the prolonged argon bombardment.[11,12] Modeling results given in Fig. 2(b) show an increase in carrier concentration as the density of these donorlike traps is increased within a thin layer at the GaAs cap surface. The results from the argon experiments represent a balance between the carrier loss in the cap layer and the creation of the donorlike damage layer. In Fig. 3, the 10-s argon exposure resulted in a loss of about 2×10^{11}/cm^2 carriers in the 2DEG. Shorter argon exposure times might have shown greater depletion. Longer times show the effect of the surface

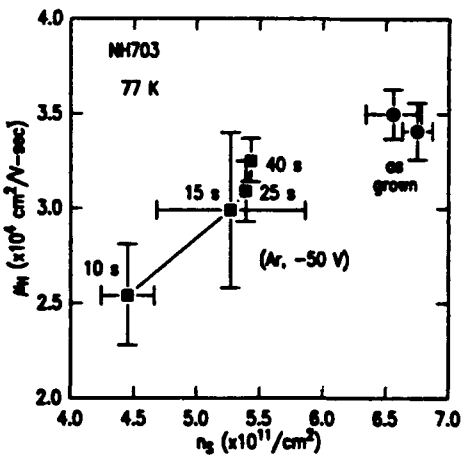

FIG. 3. The Hall mobility for the samples exposed to an argon plasma are plotted vs carrier concentration. The various exposure times are listed next to the experimental points. For these samples the effect of longer bombardment times increases the effective carrier concentration and the mobility. The as-grown values (●) are plotted as a guide.

modification with an apparent limit to the carrier increase. The mobility, however, continues to increase and approaches the value of the as-grown samples plotted as solid dots in Fig. 3. It has been suggested[12] that arsenic depletion at the GaAs surface, with the arsenic vacancies having a donor character, is responsible for the donorlike damage layer.

The sheet carrier concentration and hence the mobility of the 2DEG in heterostructure devices is critically dependent on the integrity of surface epitaxial layers.[1] It is important to understand, therefore, that even low-voltage plasmas can drastically alter the conduction of a 2DEG. Also, for some device structures, thermal processing for damage removal is not feasible, so care is recommended when employing inert gases for cleaning and buffering.

In conclusion, we have examined the damage caused by low-voltage helium and argon plasmas on an inverted heterostructure. Helium severely degraded the sheet carrier concentration and the mobility of the 2DEG at a dc self-bias voltage of only -85 V for 15 s. Argon damage was limited, with extended bombardment causing an increase in the carrier concentration and the mobility. This increase is most probably due to the creation of a thin, donorlike damage layer at the surface of the GaAs cap layer. Future studies will examine the effects of other inert gases on heterostructures containing a 2DEG.

The authors would like to acknowledge very useful discussions with J. Stasiak, T. Hickmott, T. F. Kuech, D. J. Frank, H. Hovel, and S. Tiwari, and the help of A. C. Warren for his heterostructure modeling (HETMOD) program.

[1] A. Scherer, M. L. Roukes, H. G. Craighead, R. M. Ruthen, E. D. Beebe, and J. P. Harbison, Appl. Phys. Lett. 51, 2133 (1987).
[2] M. Heiblum, D. C. Thomas, C. M. Knoedler, and M. I. Nathan, Appl. Phys. Lett. 47, 1105 (1985).
[3] C. M. Knoedler, L. Osterling, and H. Shtrikman, J. Vac. Sci. Technol. B 6, 1573 (1988).
[4] S. W. Pang, J. Electrochem. Soc. 133, 784 (1986).
[5] S. W. Pang, M. W. Geis, N. N. Efremow, and G. A. Lincoln, J. Vac. Sci. Technol. B 3, 398 (1985).
[6] H. Shtrikman, M. Heiblum, K. Seo, D. E. Galbi, and L. Osterling, J. Vac. Sci. Technol. B 6, 670 (1988).
[7] L. J. van der Pauw, Philips Res. Rept. 13, 1 (1958).
[8] C. M. Knoedler and T. F. Kuech, J. Vac. Sci. Technol. B 4, 1233 (1986).
[9] L. M. Ephrath and D. J. DiMaria, Solid State Technol. 24, 182 (1981).
[10] S. W. Pang, G. A. Lincoln, R. W. McClelland, P. D. DeGraff, M. W. Geis, and W. J. Piacentini, J. Vac. Sci. Technol. B 1, 1334 (1983).
[11] K. Yamasaki, K. Asai, K. Shimada, and T. Makimura, J. Electrochem. Soc. 129, 2760 (1982).
[12] Y.-X. Wang and P. H. Holloway, J. Vac. Sci. Technol. B 2, 613 (1984).

Transport in reversibly laser-modified $YBa_2Cu_3O_{7-x}$ superconducting thin films

Robert R. Krchnavek
Bellcore, Morris Research and Engineering Center, 445 South Street, Morristown, New Jersey 07960-1961
Siu-Wai Chan, C. T. Rogers, F. De Rosa, M. K. Kelly, P. F. Miceli, and S. J. Allen
Bellcore, Navesink Research and Engineering Center, 331 Newman Springs Road, Red Bank, New Jersey 07701-7020

(Received 22 August 1988; accepted for publication 10 October 1988)

A focused argon ion laser beam in a controlled ambient is used to modify the transport properties of superconducting $YBa_2Cu_3O_{7-x}$ thin films. The laser-modified region shows a sharp transition temperature ($T_c \approx 76$ K) that is reduced from the unmodified regions of the film ($T_c \approx 87$ K). *In situ* monitoring of the room-temperature electrical resistance is used to control the laser processing and prevent formation of the semiconducting phase. The original properties of the superconducting film can be recovered by plasma oxidation indicating that the laser-induced phase is oxygen deficient.

Electronics is a potentially important area for future applications of the high transition temperature (T_c) superconductors based on the La-Ba cuprates discovered by Bednorz and Muller,[1] and the Y-Ba cuprates discovered by Wu *et al.*[2] These potential applications will rely heavily on the ability to make and process thin films of these materials and control their local transport properties on a microscopic scale. In this communication, we report on the transport properties of superconducting $YBa_2Cu_3O_{7-x}$ films that have been locally modified by laser-induced heating in a controlled ambient. In contrast to previous work,[3–5] we demonstrate that the laser-modified film need not be driven to the insulating region of the phase diagram but may be controlled in such a way as to produce a superconducting phase with a reduced and well-defined transition temperature. This opens the possibility of controlling critical current and making weak links. Furthermore, by placing the laser-modified sample in an oxygen plasma, the original film properties can be recovered leading us to believe the laser-induced phase is oxygen deficient.

 0021-8979/89/041802-04$02.40

Lateral Tunneling, Ballistic Transport, and Spectroscopy in a Two-Dimensional Electron Gas

A. Palevski, M. Heiblum, C. P. Umbach, C. M. Knoedler, A. N. Broers,[a] and R. H. Koch
IBM Research Division, T. J. Watson Research Center, Yorktown Heights, New York 10598
(Received 7 November 1988)

We report a direct observation, via electron energy spectroscopy, of lateral tunneling and lateral ballistic electron transport in a two-dimensional electron gas (2D EG). This was accomplished through the use of a novel transistor structure employing two potential barriers, induced by 50-nm-wide metal gates deposited on a GaAs/AlGaAs selectively doped heterostructure. Hot electrons with very narrow energy distributions (≃5 meV wide) have been observed to ballistically traverse 2D EG regions ≃170 nm wide with a mean free path of about 480 nm.

PACS numbers: 73.40.Gk, 73.20.Dx

Ballistic transport of hot electrons was established recently in n^+-type GaAs by the use of energy spectroscopy in a hot-electron structure.[1] These experiments utilized an injector at one end of a transport region and a spectrometer at the other end, with the electrons moving normal to the plane of the layers (vertical transport). This technique proved to be very powerful since it permitted the energy distribution and the mean free path of the ballistic electrons to be determined. The very recent demonstration of quantized resistance in a confined quasi-two-dimensional electron gas (2D EG)[2,3] strongly suggests ballistic transport of electrons near equilibrium parallel to the interface between the layers (lateral transport). We report here the first utilization of an energy spectroscopy technique to establish *directly* lateral tunneling through an induced potential barrier and the existence of lateral ballistic transport in a 2D EG. This was done by inducing two closely spaced potential barriers in the 2D EG via two narrow Schottky metal gates deposited on the surface of the structure. One barrier was employed as a tunnel injector and the second as a spectrometer. We have measured narrow hot-electron distributions ballistically traversing lateral 2D EG regions 170 nm wide, and have estimated their mean free path.

Several structures were made on a selectively doped GaAs/AlGaAs heterostructure grown by molecular-beam epitaxy. On top of an undoped GaAs buffer layer, an undoped AlGaAs layer (50 nm thick, AlAs mole fraction $x=34\%$) was grown, followed by a thin heavily doped GaAs cap layer (15 nm thick). A sheet of Si atoms, with an areal density of $\simeq 2\times10^{12}$ cm^{-2}, was deposited under overpressure of As when growth of the AlGaAs was interrupted (planar doping), 30 nm away from the GaAs buffer layer; these supply the electrons in the 2D EG [Fig. 1(a)]. The 2D EG had a carrier density of 3×10^{11} cm^{-2} and a mobility of 3×10^5 cm^2/V sec at 4.2 K. Two parallel AuPd gates, each 52 nm wide and 0.5 μm long, were patterned 93 nm apart using electron-beam nanolithography, on a 5-μm-wide isolated 2D EG line [Fig. 1(b)]. Ohmic contacts were made to the three regions defined by both gates. Biasing the gates negatively with respect to the central region between them (called the base) depleted the 2D EG underneath the gates and prevented the free motion of the equilibrium electrons among the three regions [emitter (E), base (B), and collector (C)]. The potential barriers shown in Fig. 1(a) give an approximate guide to the potential shape for different gate voltages (which are about −0.5 V). The separation between the Fermi level, E_F, and the conduction band outside the base is 10.7 meV. In the base this separation can be substantially smaller, and the actual conductive width of the base (always smaller than the geometrical separation between the gates) was roughly estimated to be, for example, 70 nm when both barriers were 10 meV above the Fermi level [Fig. 1(a)]. Since this distance is similar to the average electron Fermi wavelength in the base, the base electrons are expected to be quasi-one-dimensional.

With no applied gate voltages, the measured resistances at 4.2 K among all three terminals (E, B, and C) were a few kilohms and constant with the applied terminal voltage. As the emitter- (or collector-) gate voltage, V_{GE} (or V_{GC}) was made negative with respect to the base (which was the reference in all our measurements), the emitter current, I_E, supplied by a source V_{EB} (or the collector current, I_C, supplied by a source V_{CB}) decreased. For gate voltage V_{GE} (or V_{GC}) < -0.4 V the resistance under the gate became very nonlinear and approached 10^8–10^9 Ω at low voltage (shown by I_E vs V_{EB} in Fig. 2). Simple WKB calculations of the tunneling currents through square barriers 50 nm wide and 20 meV high, resembling our barriers, resulted in similar tunneling resistances. The occurrence of tunneling through the barriers will be revisited and verified later in more detail. When only the emitter barrier was formed ($V_{GE} < -0.4$ V, $V_{GC}=0$), the emitter current I_E, which resulted from a negative V_{EB}, split into I_B and I_C in the ratio of the base and collector resistances of the 2D EG (note that $V_{CB}=0$ V). When the spectrometer barrier was also induced ($V_{GE} < -0.4$ V, $V_{GC} < -0.4$ V), the current in the collector remained practically zero (and $I_B=I_E$) until $|V_{EB}|$ exceeded a certain value (collector-current onset value). Thereafter it increased sharply. As seen in Fig. 2, the onset value increased as $|V_{GC}|$ increased and was similarly affected by an applied small V_{CB}. These

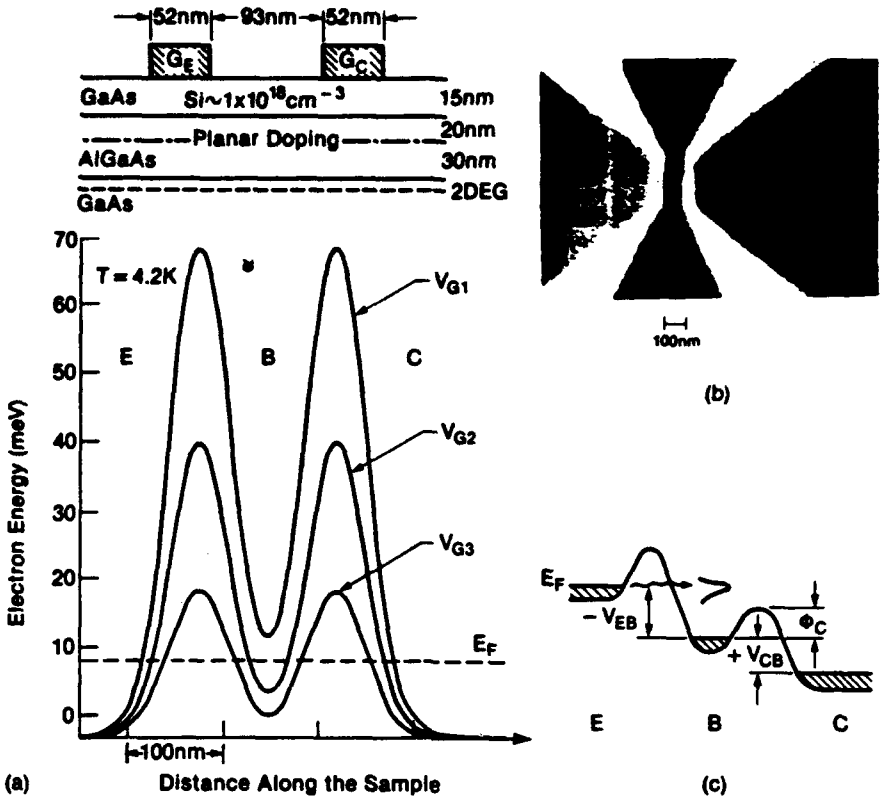

FIG. 1. (a) A cross-sectional cut showing the selectively doped structure and the gates on top. Underneath is plotted the potential shape in the lateral direction showing injector and spectrometer barriers. As V_G became more negative the potential barrier increased. (b) A scanning electron micrograph showing the gate configuration. (c) A schematic description of the potential distribution for a biased device, $V_{EB} < 0$ and $V_{CB} > 0$.

observations, which clearly resulted from changes in the spectrometer barrier height, Φ_C, demonstrate that the abrupt onset of I_C is due to energetic electrons that surmount the spectrometer barrier potential [see Fig. 1(c)]. Considering the small distance between injector and spectrometer barriers, a fraction of the electrons injected from the Fermi level in the emitter was expected to traverse the base ballistically, leading to collector-current onset at $eV_{EB} = \Phi_C$, where Φ_C is the collector barrier height. This allowed us to measure Φ_C, a result we can use to further verify the existence of ballistic transport and find the actual fraction of ballistic electrons arriving at the collector.

We have performed electron energy spectroscopy[1,4,5] by varying the spectrometer barrier height Φ_C with V_{CB}. The collected current is given by $I_C = A\int_{\Phi_C}^{\infty} en(E) \times v(E)dE$, where A is the area, $n(E)$ is the energy distribution of the electrons arriving at the spectrometer, and E and v are the energy and velocity associted with the electrons traversing normal to the gates. In a small enough energy range $v(E)$ is fairly constant, and the electron energy distribution can be described by $n(E) \propto dI_C/d\Phi_C$ for a constant injection energy, eV_{EB}. The same expression can be rewritten as $n(E) \propto (dI_C/deV_{CB})(deV_{CB}/d\Phi_C)$. Figure 3(a) (solid lines) shows a typical family of I_c vs V_{CB} characteristics for $V_{GE} = V_{GC} = -0.5$ V and different injection energies, all chosen to be higher than the unbiased spectrometer barrier height (for $V_{EB} = 0$ V, $I_C = 0$ in the range of interest). For $V_{CB} > 0$, the collector current increased only slowly as V_{CB} increased, suggesting that most of the hot electrons had energies higher than the unbiased potential barrier height. When the polarity of V_{CB} was reversed, leading to an increase in Φ_C, the collector current decreased slowly initially, followed subsequently by a sharp drop to zero over a range of a few mV. This behavior indicates that electrons with a narrow energy distribution were cut off by the spectrometer barrier. Before elaborating more on the shape of the energy distribution we would like to note that for injector barrier heights smaller than some 20 meV ($V_{GE} > -0.5$ V) the behavior was quite different, as shown for two lower injector barrier heights [dotted lines in Fig. 3(a)]. The collector currents became zero at the same negative V_{CB} (and thus the same Φ_C) for the three cases. This indicates that, even though the nature of the injection in each case may have been different, the highest energy of the injected and collected electrons was always determined by eV_{EB}. The absence of a "knee" observed for the lower injector barriers indicates that the injected distributions were broad, extending from the injection energy eV_{EB} and below, and were not the result of tunneling. It is quite possible that

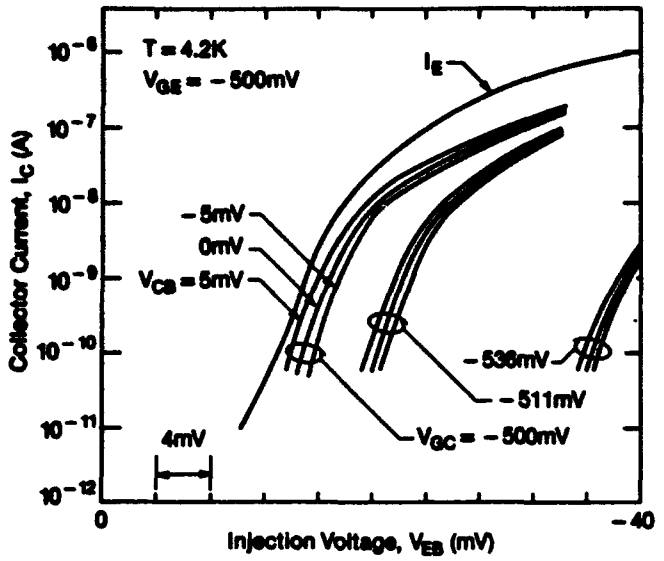

FIG. 2. The collector current I_C as a function of the injection voltage V_{EB} when the collector-gate voltage V_{GC} and the collector-base voltage V_{CB} serve as parameters. The current onset, indicative of the collector barrier height, is strongly influenced by both parameters. The injected current I_E is independent of the parameters.

when the injector barrier was low, the application of an injection voltage removed the barrier completely, or made it so narrow that the injected electron distributions were very broad.

To determine the collected energy distributions one has to change the energy scale from eV_{CB} to the corresponding height of the spectrometer barrier Φ_C, and multiply the dI_C/deV_{CB} curves by the $deV_{CB}/d\Phi_C$. The barrier heights $\Phi_C(V_{CB})$ and the factor $deV_{CB}/d\Phi_C$, summarized in Fig. 3(b), were found from collector-current onset measurements in a similar way to that described before. The energy distributions shown in Fig. 3(c) have a full width at half maximum of about 5 meV, which tended to increase as the injection energy increased [up to 10 meV for eV_{EB} = 30 mV (not shown)]. The peaks of the distributions shifted with the same energy as that of injection energy (except the lowest one which was obscured by the lower-energy tail), as expect-

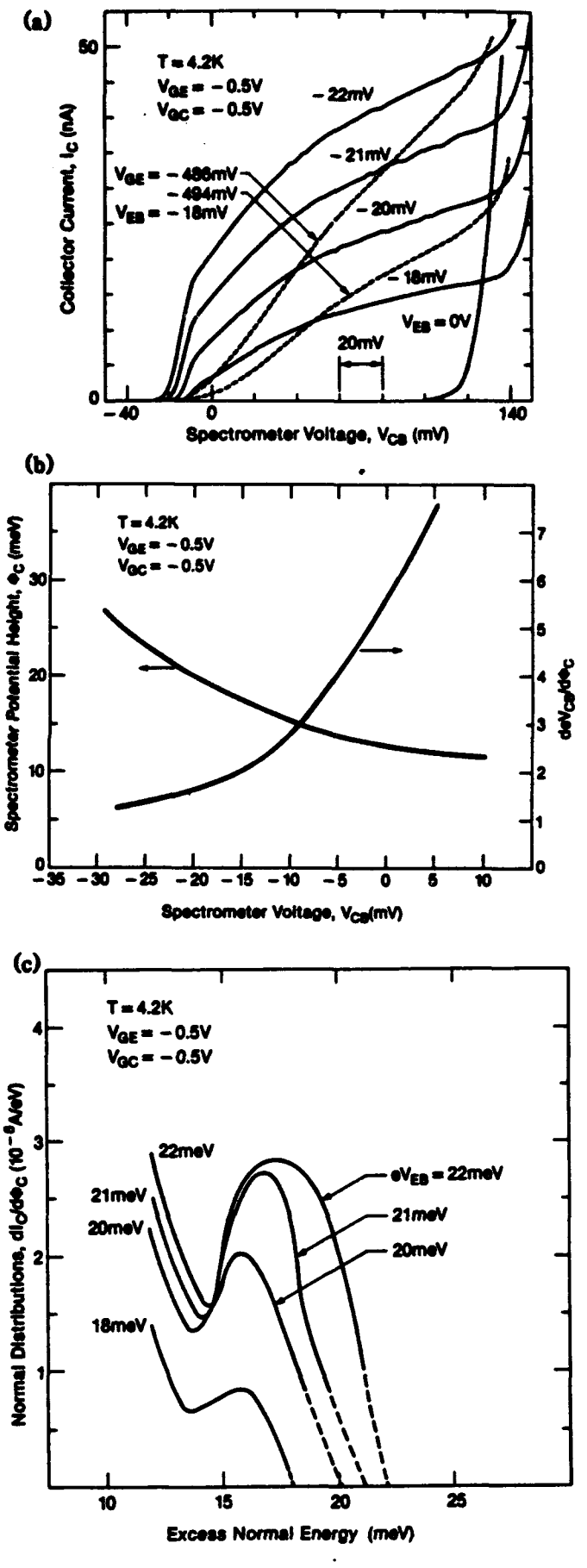

FIG. 3. (a) The family of the collector-current characteristics where I_E = 0, −20, −40, −60, −80 μA. Note the sharp rise in the current (for V_{CB} = −10 mV) followed by a moderate rise indicative of a narrow ballistic distribution. The dotted lines are for lower injector barrier heights and for eV_{EB} = −18 mV, where the injected distributions were very broad. (b) The spectrometer barrier height determined by measuring the collector-current onsets, and the $deV_{CB}/d\Phi_C$ deduced from it. (c) The ballistic distributions for different injection energies as a function of excess normal energy above the Fermi level in the base. The peaks of the distributions follow rigidly the injection energy. At higher $|V_{CB}|$ leakage currents dominated.

ed in ballistic transport. The peak energies, which were lower by about 3–4 meV than the corresponding Fermi level in the emitter (noted by the crossing of the dotted lines with the energy axis), and the narrow distribution width (≃5 meV) were both expected for the normal energy distributions injected by 50-nm-wide, 20-meV-high tunnel barriers.[6] These results proved that tunneling was the injection mechanism in our induced barriers. At their lower-energy tails the distributions rise again, most probably due to lower-energy electrons that are excited from the Fermi sea in the base by scattered (nonballistic) electrons.[4] Even though small-angle elastic-scattering events cannot be excluded, the similarity of the results presented here with the results that confirmed ballistic transport in vertical structures,[1] as well as the narrow width of the electron distributions, strongly suggests that elastic scattering in our lateral structures was minimal.

The ballistic fraction, α, is defined as the ratio between the number of ballistic electrons collected (the ballistic current is I_C at $V_{CB}=0$ or the area under the distribution) and the total number of injected electrons (the injected current I_E). From Fig. 3(a) we find $I_C/I_E \simeq 0.25$ at $V_{CB}=0$, which is approximately the ballistic fraction collected. Since some of the injected current emerged from the periphery of the injector barrier (where the separation between them increases) and never surmounted the spectrometer barrier, the value 0.25 was not appropriate to use for the calculation of the ballistic mean free path (λ). To minimize the number of these "stray" electrons, different structures where the collector gate was 3 times longer (0.75 μm) than the emitter gate (0.25 μm) were made (base width 170 nm). Carrying out energy spectroscopy in these devices, ballistic fractions higher than 0.7 (Ref. 7) were measured. Using $\alpha=\exp(-d_B/\lambda)=0.7$, where d_B is the effective base width for the hot electrons, we find $\lambda \simeq 480$ nm. This lower limit on λ suggests that the mean free path of the hot electrons is on the same order as that of cold electrons. This might result in part from the relatively low density of electrons in the base and from size quantization effects in the quasi-one-dimensional base that may reduce the scattering cross sections.[8]

Since tunneling occurred into a quantized base, we have looked for, but did not observe, resonant tunneling effects in the injection currents.[9] Upon increasing the injection energy, but keeping $e|V_{EB}|<\Phi_C$, we had expected to see an enhancement in the injected current when the Fermi level in the emitter crossed a bound state in the base. To get a rough idea of the expected positions of the states, we modeled our double-barrier potential with a sine function, having a peak-to-peak value of 30 meV and a period of 140 nm. The solutions, which involved Mathieu functions,[10] predicted two states under the Fermi level (3 and 8.6 meV), and five states above (14, 19, 23.5, 27, and 29.5 meV). Since emitter currents could be measured only for $V_{EB}<-(10\text{–}15)$ mV, only the highest two states (near the continuum) could in principle have been observed. Because of the finite width of the distribution (≃5 meV) it would be difficult to resolve these states from the continuum. In cases of lower barrier heights the energy separation between the states was expected to be even smaller and their energy width wider, making observation difficult.

In summary, we have seen for the first time, lateral tunneling through narrow potential barriers induced by thin gates, and ballistic hot-electron transport with a long mean free path, in a two-dimensional electron-gas (2D EG) channel. Via the utilization of an energy spectroscopy technique, narrow electron distribution injected by a tunneling barrier were detected, establishing directly ballistic transport and tunneling injection. We estimate a ballistic mean free path for hot electrons of about 0.48 μm.

We would like to thank L. Osterling for his help with the molecular-beam-epitaxy growth, M. Weckwerth for his help with processing, P. M. Soloman and F. Stern for useful discussions, and T. W. Hickmott, C. J. Kircher, and S. Washburn, for their comments on the manuscript. One of us (A.P.) would like to thank R. B. Laibowitch for his continuous support. The work was partly supported by the U.S. Defense Advanced Research Projects Agency and administered by ONR, Contract No. N00014-87-C-0709.

---

[a]Permanent address: Department of Engineering, Cambridge University, Cambridge, England.

[1]M. Heiblum, M. I. Nathan, D. C. Thomas, and C. M. Knoedler, Phys. Rev. Lett. 55, 2200 (1985).

[2]D. A. Wharam, T. J. Thornton, R. Newbury, M. Pepper, H. Ahmed, J. E. F. Frost, D. J. Hasko, D. C. Peacock, D. A. Ritchie, and G. A. Jones, J. Phys. C 21, L209 (1988).

[3]B. J. van Wees, H. van Houten, C. W. J. Beenakker, J. G. Williamson, L. P. Kouwenhoven, D. van der Marel, and C. T. Foxon, Phys. Rev. Lett. 60, 848 (1988).

[4]M. Heiblum, K. Seo, H. P. Meier, and T. W. Hickmott, Phys. Rev. Lett. 60, 828 (1988).

[5]D. J. Dimaria, M. V. Fischetti, J. Batey, L. Dori, E. Tierney, and J. W. Stasiak, Phys. Rev. Lett. 57, 313 (1986).

[6]M. Heiblum, D. Galbi, and M. Weckwerth, Phys. Rev. Lett. 62, 1057 (1989); K. Seo (private communication).

[7]When emitter and collector were reversed in the asymmetric device, the ballistic fractions decreased approximately by the ratio between the gate lengths (1:3); another indication of the straight trajectories of the electrons in their ballistic motion. This work will be published later.

[8]D. C. Herbert (private communication).

[9]M. Heiblum, M. V. Fischetti, W. P. Dumke, D. J. Frank, I. M. Anderson, C. M. Knoedler, and L. Osterling, Phys. Rev. Lett. 58, 816 (1987).

[10]*National Bureau of Standards, Tables Relating to Mathieu Functions* (Columbia Univ. Press, New York, 1951).

High-gain lateral hot-electron device

A. Palevski, C. P. Umbach, and M. Heiblum
IBM Research Division, T. J. Watson Research Center, Yorktown Heights, New York 10598

(Received 17 April 1989; accepted for publication 24 July 1989)

A lateral hot-electron device has been fabricated in a plane of a two-dimensional electron gas. The transfer ratio of the device, α, was studied for different geometrical configurations of the emitter barrier. The maximum transfer ratio was greater than 0.99 at 4.2 K, corresponding to a current gain greater than 100 for devices with base widths of 220 nm. An emission of a single longitudinal optical phonon, by the injected electrons, has been observed.

The tunneling hot-electron transfer amplifier (THETA) is a low-gain ballistic device.[1,2] Although it is a unipolar device its behavior is similar to a bipolar transistor. Because of its vertical configuration the device has some drawbacks: it is difficult to form low-resistance ohmic contacts to the narrow (~30 nm) base avoiding shorting of base and collector, it is difficult to expose the buried base avoiding its depletion, and it is difficult to obtain high gain because of the short ballistic mean free path (mfp) in the heavily doped base. To circumvent some of these problems we proposed and fabricated a novel hot-electron device (a "lateral THETA" device[3]) in the plane of a two-dimensional, high-mobility electron gas (2DEG). The characteristics of this lateral device are similar to those of the vertical device, but it is easier to fabricate. The device is expected to have a higher gain due to the longer mfp of hot electrons in the plane of the 2DEG. We report here on the realization of lateral hot-electron devices with a 4.2 K current transfer ratio α greater than 0.99, for base widths greater than 200 nm. We look in some detail at the injection properties of our lateral injector and also observe single phonon emission by the hot electrons.

In the vertical THETA device[4] a tunnel barrier injector emits a fairly monoenergetic hot-electron beam into the base. After their traversal through the base, the electrons surmount another thick potential barrier. This barrier prevents the equilibrium electrons that reside in the base from entering the collector. Since the collector current is only slightly affected by the shape of the collector barrier (if quantum mechanical reflections are small), the current transfer ratio is almost independent of the collector voltage and the output differential resistance can be large, as desired for device applications.

In order to make a lateral THETA device, two narrow barriers separated by a thin base were constructed in the plane of a GaAs-$Al_{0.3}Ga_{0.7}As$ selectively doped heterojunction. The 2DEG had a carrier density of $n_s \simeq 2.0\times10^{11}$ cm^{-2} and a mobility $\mu \simeq 7.5\times10^5$ cm^2/V s at 4.2 K. Utilizing nanolithography two narrow metal gates, each about 50 nm long, were deposited on the surface of the heterojunction (length is the dimension along the current path, as seen in Fig. 1). In a variety of devices the emitter gate G_E was made 0.25–1 μm wide and the collector gate G_C was made 0.75–1 μm wide, wider than the emitter gate in order to collect all of the ballistic electrons. The three regions defined by the two gates, emitter (E), base (the central region B), and collector (C) were contacted with NiAuGe alloyed ohmic contacts. An application of a sufficiently negative gate voltage, V_{GE} (or V_{GC}), with respect to the 2DEG depletes the electrons underneath the gate, forming thus a potential barrier for the electrons residing on both sides of the gate. Inducing two potential barriers, with the two gates shown in Fig. 1, enables us to reproduce, in the lateral plane, a potential distribution similar to that of the vertical hot-electron device. Using the emitter barrier as a tunnel injector produces a hot-electron distribution ~5 meV side.[5] Quantum mechanical reflections from the collector barrier are negligible because of the slow change of the collector barrier potential. Scattering events in the base are expected to be few due to the lower dimensionality of the base[6] and the absence of nearby impurities. Note that the tunneling currents through the wide parts of the emitter and collector gates (see Fig. 1) can be ignored, thus contacting the 2DEG in the narrow base region is established by contacting the remote, external parts of the base.

We have recently reported results of energy spectroscopy experiments made on a lateral THETA device. There we found the transport to be ballistic with ballistic distributions 3–5 meV wide.[3] In symmetric structures where the width of the emitter and the collector gates is similar, the electrons emerging from the edges of the injector, not perpendicularly

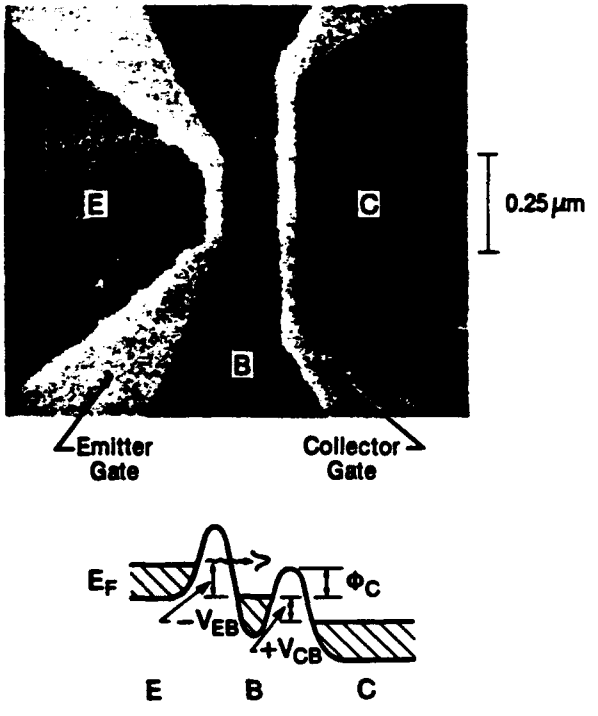

FIG. 1. Scanning electron microscopy micrograph of the lateral THETA device and a schematic description of a potential distribution for a negatively biased emitter and a positively biased collector.

 0003-6951/89/401421-03$01.00

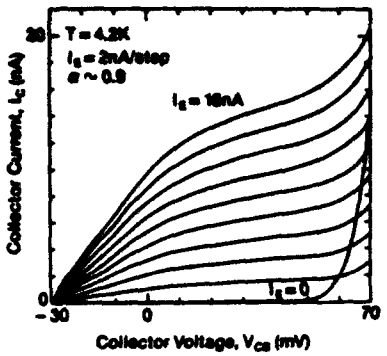

FIG. 2. Output I-V characteristics of the lateral device in a common base configuration. The emitter gate width is 0.25 μm, the collector gate width is 0.75 μm, and base length is 0.17 μm.

to the gates, are not collected. Indeed, in these symmetric devices, the transfer ratio $\alpha \equiv I_C/I_E$, where I_C and I_E are the collector and the emitter currents, respectively, was only 0.4 at 4.2 K.[3] To alleviate this problem a device with emitter and collector gate widths of 250 and 750 nm, respectively, and a base length of 170 nm, was made (Fig. 1). The measured output characteristics in a common base configuration are shown in Fig. 2, demonstrating a transfer ratio $\alpha = 0.9$ over a large range of injected currents and collector voltages. The ballistic fraction of the collected current, α_B, is measured at a collector to base voltage V_{CB} where the collector current I_C almost saturates ($V_{CB} \simeq 20$ mV).[3] Using $\alpha_B = \exp -d_B/\lambda = 0.7$, where d_B is the base width, we find a mfp, $\lambda \simeq 480$ nm. The true mfp is longer since some of the injected electrons emerging from the edges arrive at the collector with a low normal energy component and thus are not collected.

The solid line in Fig. 3 shows a typical dependence of α on the injection energy eV_{EB} for fixed emitter and collector barrier heights. The existence of a maximum value α_{max} is characteristic for these types of curves. In general we expect to see a monotonic increase in α due to the increasing group velocity of the ballistic electrons and the reduction of scattering cross sections as the kinetic energy of the electrons increases. Also, a larger fraction of the ballistic distribution will surmount the collector barrier.[5] The drop in α observed at higher V_{EB} is due to the relative increase of the side-tunneling current. This can be seen from the Wentzel–Kramers–Brillouin expression for the tunneling probability $D \propto \exp[-A(\phi^{3/2}w/V)]$, where A is a constant, ϕ is the emitter barrier height, w is a barrier width, and V is the applied injection voltage. From here, the ratio of the tunneling probabilities through two barriers with different widths w_1 and w_2 is $D_1(w_1)/D_2(w_2) = \exp[-A\phi^{3/2}(w_1 - w_2)/V]$, explaining the relative increase of the side currents and the drop in α beyond α_{max}. As the emitter potential barrier increases, the side currents become substantial only at higher values of injection voltages, moving thus α_{max} to higher V_{EB}'s. The increasing part of the transfer ratio curve for all emitter barrier heights, displayed in Fig. 3 (up to the maximum on the solid line) however, is not affected by the side currents.

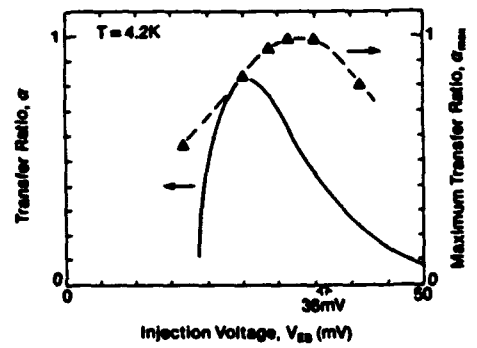

FIG. 3. Variation of the transfer ratio α with the injected voltage (a solid line) at a fixed value of the emitter gate voltage. The dashed line shows the behavior of α_{max} (extracted from a few curves of α).

Plotting the measured α_{max} for different emitter barrier heights versus V_{EB} in Fig. 3 (a dashed line) recovers the behavior of α vs V_{EB} in the absence of any side tunneling and at approximately the same injected currents. The interesting feature of the plot is the maximum reached by α_{max} (>0.98) at energies just below 36 meV. The drop in α for injection energies that exceed $\simeq 36$ meV is due to an emission of a longitudinal optical (LO) phonon (already observed in thin GaAs layers[5]). The high value of α_{max} measured here for $V_{EB} < 36$ mV suggests that LO-phonon emission is the dominant relaxation mechanism of hot electrons in a high-mobility 2DEG.

To eliminate side-tunneling currents altogether we have modified the injector structure. Two gates, each 65 nm wide separated by ~ 600 nm, were added in the emitter region as shown in the insert of Fig. 4(a). Since the emitter current is now confined to flow between these negatively biased gates (with voltage V_{GG} applied relative to base) without reaching the emitter gate corners, side-tunneling currents are prevented. Figure 4(a) shows the behavior of α for different side-gate potentials. As the negative side-gate bias increases up to -0.55 V, α increases. However, for a bias -0.6 V or greater α does not increase anymore indicating the elimination of side tunneling. A more sensitive measurement of this increase can be obtained by measuring the current gain $\beta \equiv \alpha/(1-\alpha)$, as shown in Fig. 4(b). At $V_{GG} = -0.55$ V, β exhibits pronounced maxima which move towards higher values of V_{EB} as the emitter barrier height increases. The drop in the gain for higher injection voltages is somewhat surprising since side currents have been eliminated. In a closer look we find that the gain always reaches its maximum when the injection current reaches approximately 100 nA, corresponding to a current density of $\sim 3 \times 10^3$ A cm^{-2} in the 2DEG. This is found to be the case for all emitter barrier heights and for all values of α_{max}. This observation might suggest that the decrease in the gain is related to the current density being higher than some critical value. Although this phenomenon is not yet understood, it is plausible that at a sufficiently high current density charging of the collector barrier region becomes important leading to an increase in the barrier height and to the observed reduction in the gain.

The maximum value of β is found to be as high as 105, corresponding to $\alpha > 0.99$. This is the highest current gain ever reported in a hot-electron device. The large value of the transfer ratio does not necessarily imply that the mfp is that long. At sufficiently high injection voltage the electrons are injected at energies much higher than the collector barrier

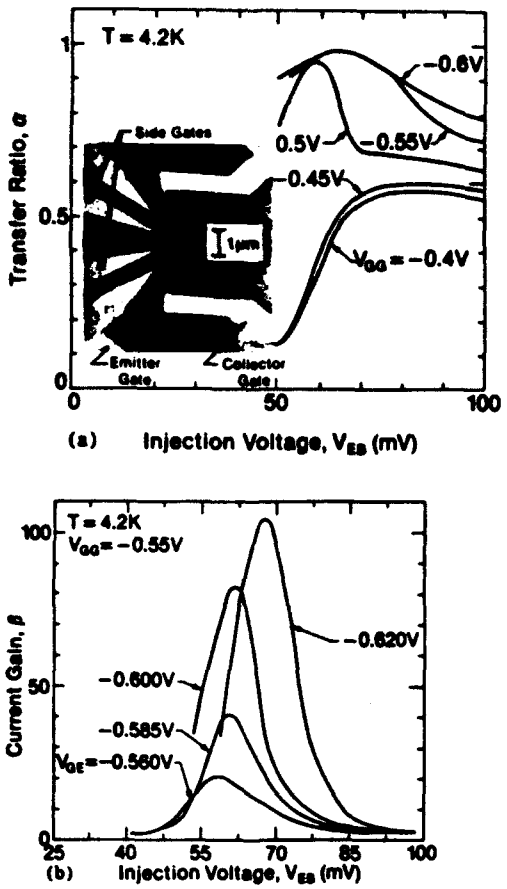

FIG. 4. (a) Effect of the side gates (inset), biased V_{GG} with respect to base, on the transfer ratio. (b) The variation of the current gain with the injection voltages V_{EB} for different emitter gate voltages in the absence of side-tunneling current.

height (which is about 20–30 meV high). Hence, they may lose a part of the normal energy component as a result of inelastic or elastic scattering and still be collected by the collector.

Our side gates can be used not only to eliminate side-tunneling currents but also to narrow the width of the emitter channel and eventually to pinch off the injector. The narrowing of the channel should result in increasing of transverse momentum components due to size quantization effects. This eventually should lead to the reduction of the current gain. We indeed observe a decrease in the gain when the channel is narrowed substantially (not shown). The maximum current gain β drops by a factor of ~ 2.5 as the side gates voltage varies from -0.55 to -0.7 V.

In conclusion, we have looked in some detail at the characteristics of a lateral hot-electron device fabricated on the plane of a high-mobility 2DEG. The high mobility of the 2DEG enabled a long mfp of the ballistic hot electrons below the LO-phonon energy. Current gains greater than 100 were measured. The possibility to tune the emitter and collector barrier heights, which are induced by submicron metallic gates, makes the device extremely powerful for studying ballistic transport and relaxation mechanisms in small systems.

We thank L. Osterling and H. Shtrikman for their contribution in the molecular beam epitaxy growth, and P. Solomon and U. Sivan for useful discussions. The work was partly supported by Defense Advanced Research Projects Agency and administered by Office of Naval Research contract No. 00014-87-C-0709.

[1]K. Seo, M. Heiblum, C. M. Knoedler, J. Oh, J. Pamulapati, and P. Bhattacharya, IEEE Electron Device Lett. 10, 73 (1989).
[2]K. Imamura, S.-i. Muto, and N. Yokoyama, Fujitsu Sci. Tech. J. 24, 54 (1988).
[3]A. Palevski, M. Heiblum, C. P. Umbach, C. M. Knoedler, R. Koch, and A. Broers, Phys. Rev. Lett. 62, 1776 (1989).
[4]M. Heiblum, Solid-State Electron. 24, 343 (1987).
[5]M. Heiblum, D. Galbi, and M. Weckwerth, Phys. Rev. Lett. 62, 1057 (1989).
[6]D. C. Herbert, Semicond. Sci. Technol. 3, 1129 (1988).